AWARD NUMBER: W81XWH-15-1-0190

TITLE: Neurosteroids Reverse Tonic Inhibition Deficits in Fragile X Syndrome

PRINCIPAL INVESTIGATOR: Dr. Paul A. Davies

CONTRACTING ORGANIZATION: Tufts University School of Medicine
136 Harrison Ave
Boston MA 02111-1817

REPORT DATE: October 2017

TYPE OF REPORT: Final

PREPARED FOR: U.S. Army Medical Research and Materiel Command
Fort Detrick, Maryland 21702-5012

REPORT DOCUMENTATION PAGE

Form Approved
OMB No. 0704-0188

1. REPORT DATE	2. REPORT TYPE	3. DATES COVERED
October 2017	Final	15 July 2015 – 14 July 2017

4. TITLE AND SUBTITLE

Neurosteroids Reverse Tonic Inhibition Deficits in Fragile X Syndrome

5a. CONTRACT NUMBER

5b. GRANT NUMBER
W81XWH-15-1-0190

5c. PROGRAM ELEMENT NUMBER

6. AUTHOR(S)
Dr Paul A. Davies

E-Mail: paul.davies@tufts.edu

5d. PROJECT NUMBER

5e. TASK NUMBER

5f. WORK UNIT NUMBER

7. PERFORMING ORGANIZATION NAME(S) AND ADDRESS(ES)

Tufts University School of
Medicine
136 Harrison Ave
Boston MA 02111-1817

8. PERFORMING ORGANIZATION REPORT NUMBER

9. SPONSORING / MONITORING AGENCY NAME(S) AND ADDRESS(ES)

U.S. Army Medical Research and Materiel Command
Fort Detrick, Maryland 21702-5012

10. SPONSOR/MONITOR'S ACRONYM(S)

11. SPONSOR/MONITOR'S REPORT NUMBER(S)

12. DISTRIBUTION / AVAILABILITY STATEMENT

Approved for Public Release; Distribution Unlimited

13. SUPPLEMENTARY NOTES

14. ABSTRACT
Our preliminary studies demonstrate that Fmr1 KO mice at p21 have a decrease in phosphorylation of S443 in the α4 subunit compared to WT and an increase in the phosphorylation of β3 subunits at the S408/409 site compared to WT. We have previously showed that phosphorylation of these residues changes the trafficking of the subunits so the changes observed in Fmr1 KO mice would predictably have consequences for trafficking of these essential inhibitory subunits. We noted that there was a significant decrease in tonic inhibition in dentate gyrus granule cells in p21 Fmr1 KO mice compared to WT. A 10 min exposure to neuroactive steroids followed by a 30 min wash induced a >3 fold increase in tonic current in Fmr1 KO animals which was prevented with PKC inhibition. Using a perforated multi-electrode array we have observed in cortical-hippocampal slices seizure like events (SLE) propagating through the dentate gyrus and into the CA3 and CA1 regions of the hippocampus of Fmr1 KO mice but in WT mice SLEs did not propagate through the dentate gyrus. We predict the increase neuronal excitability seen in Fmr1 KO mice is due to the deficits in tonic inhibition.

15. SUBJECT TERMS
GABA receptor, protein kinase C (PKC), Neuroactive steroid, tonic inhibition, dentate gyrus, seizures

16. SECURITY CLASSIFICATION OF:			17. LIMITATION OF ABSTRACT	18. NUMBER OF PAGES	19a. NAME OF RESPONSIBLE PERSON
a. REPORT	b. ABSTRACT	c. THIS PAGE			USAMRMC
Unclassified	Unclassified	Unclassified	Unclassified	42	19b. TELEPHONE NUMBER *(include area code)*

Table of Contents

Page

1. Introduction

Fragile X syndrome (FXS) is the most common form of inherited intellectual disability. In addition, there is increased incidence of anxiety, sleep irregularities, and seizure activity. The underlying cause of FXS is a loss of the fragile X mental retardation protein (FMRP). Studies from both FXS patients and animal models have revealed reduced expression levels of extrasynaptic $GABA_AR$ α4 and δ subunits with a reduced efficacy of tonic inhibition. Neuro-active steroids (NAS) are known allosteric modulators of $GABA_AR$ channel function but recent studies from our laboratory have revealed that NAS also exert persistent effects on the efficacy of tonic inhibition by increasing the PKC-mediated phosphorylation of the α4 subunit which increases the membrane expression and boosts tonic inhibition. We have used a combination of biochemical and electrophysiological methods to assess alterations in GABAergic signaling in the hippocampus of FMRP knock-out mouse (*Fmr1 KO*), a widely validated model of the human syndrome. In addition, we propose an innovative way of reversing the reduced tonic inhibition by boosting $GABA_AR$ trafficking to produce a sustained increase in tonic current with the use of NASs including a novel NAS which has improved bioavailability, and pharmacokinetic properties.

2. Keywords

GABA receptor, protein kinase C (PKC), Neuroactive steroid, tonic inhibition, dentate gyrus, seizures

3. Accomplishments

What were the major goals of the project?

Specific Aim 1: Determine the phosphorylated state and cell surface accumulation of $GABA_AR$ subunits in FXS mice and the role of neurosteroids in altering subunit expression.

1. To analyze the NS-mediated changes in phosphorylation of $GABA_ARs$.
2. To test the role that NS exposure plays in regulating the cell surface stability of $GABA_ARs$.

Specific Aim 2. Determining exposure to neurosteroids enhances the efficacy of tonic inhibition in FXS.

1. Measure the efficacy for NS to rescue the deficits of tonic inhibition in *Fmr1 KO* mice.
2. Characterize the changes to phasic inhibition in dentate gyrus from *Fmr1 KO* mice.
3. To examine the deficit of tonic inhibition on circuit excitability in *Fmr1 KO* mice compared to WT and impact of NS treatment.

Specific Aim 3. Ascertaining behavioral phenotypes in *Fmr1 KO* mice will be reversed with NS exposure.

1. To examine audiogenic seizures in *Fmr1 KO* mice following NS treatment.
2. To compare inappropriate social behavior in *Fmr1 KO* and WT mice.

- Milestone #1: Manuscript on the findings from the study. 18-24 months of study.

What was accomplished under these goals?

We have published our findings on phosphorylation of S408/409 residues on the β3 subunit in the *Fmr1 KO* mouse in Vien et al., 2015. The β3 subunit, along with α4 subunits, are major subunits contributing to extrasynaptic $GABA_A$Rs. Phosphorylation of these residues decreases the endocytosis of $GABA_A$Rs containing the β3 subunit. We assessed the importance of these residues by creating a mouse with the residues mutated to alanines (S408/9A) which also reduces endocytosis. The mouse exhibited autistic like properties such as increased repetitive behavior, decreased social interaction, and altered dendritic spine morphology. Because of the comorbidity of seizures in autism we examined seizure activity in the S408/9A mouse. The mice exhibited increase sensitivity to kainic acid-induced seizures. Similar to our preliminary findings in the *Fmr1 KO* mouse, the S408/9A mouse also had reduced tonic currents and increased phasic currents in dentate gyrus granule cells. Furthermore, we observed a decrease in α4 subunit immunoreactivity in hippocampal sections from S408/9A mouse. These data demonstrate that

changes in the phosphorylation of β3 subunits can alter $GABA_AR$ expression and contribute to the pathophysiology of autistic spectrum disorders.

Specific Aim 1. ***Determine if the alterations in the phosphorylation state of $GABA_AR$ subunits in Fmr1 KO mice impacts the cellular distribution within the hippocampus. (PI: Moss).***

Fmr1 KO **mice have age dependent alterations in hippocampal $GABA_AR$ subunit phosphorylation and expression.** We have previously reported a reduction in the $GABA_AR$-mediated tonic current recorded from hippocampal dentate gyrus neurons. To assess if these modifications reflect alterations in the phosphorylation and/or stability of $GABA_ARs$, we compared these parameters in hippocampal slices from both WT and *Fmr1 KO* genotypes. We examined the phosphorylation of S443 in the α4 subunit, in addition to S408/9 in the β3 subunit. These residues are accepted substrates of PKC and their phosphorylation plays key roles in regulating the membrane trafficking of $GABA_ARs$. In the case of S443 its phosphorylation acts to increase insertion of α4 subunit containing $GABA_ARs$ receptors into the plasma membrane and sustained increase in tonic inhibition. In contrast, phosphorylation of S408/9 acts to reduce receptor endocytosis increasing their accumulation at inhibitory synapses (Abramian et al 2014, Abramian et al 2010, Adams et al 2015).

Hippocampal slices from both genotypes were immunoblotted with an α4 subunit antibody to measure total levels, and a phospho-specific antibody produced against S443 (pS443), which was raised in rabbits against a synthetic peptide derived from the murine α4 subunit in which S443 was phosphorylated (PGSLGSA**S**TRPA). For the β3 subunit, samples were blotted with pS408/9 and β3 subunit antibodies as detailed previously (Jovanovic et al 2004). The ratios of pS443/α4 and pS408/9/β3 subunit immunoreactivity were compared between genotypes. We also examined the phosphorylation of S383 in the β3 subunit, which is a substrate of CamKII, but not PKC, using the respective phospho-specific antibody pS383 (Saliba et al 2012).

To measure the expression levels of $GABA_A$Rs that mediate phasic inhibition we measured levels of the α1, α2 and γ2 subunit, and for tonic inhibition we employed antibodies against the α4, α5 and δ subunits. The levels of the receptor β1, β2 and β3 subunits that are components of subtypes that mediate both forms of GABAergic inhibition were also compared between genotypes.

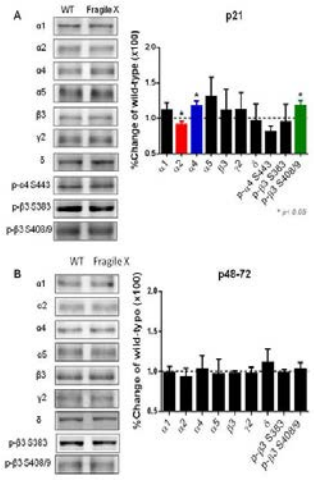

Figure 1. Comparison of $GABA_AR$ expression and phosphorylation in Fmr1 KO mice. *50 μg of SDS-soluble hippocampal extracts from (**A**) p21, (**B**) p48-72 C57/BI6 Fmr1 KO mice, or WT controls were subject to immunoblotting with antibodies against the $GABA_AR$, α1, α2, α4, α5, β3, γ2 and δ. Total subunit expression levels were then normalized to WT. In addition, extracts were immunoblotted with p-α4 S443, p-β3 S408/9 and p-β3 383 antibodies. The ratios of pS409/9/β3 and pS383/β3 immunoreactivity were compared and normalized to values seen in WT mice. * = significantly different to control p<0.05 (t-test; n=3-8 mice).*

Using immunoblotting we compared the expression levels and phosphorylation of $GABA_A$R subunits in *Fmr1 KO* mice. We measured these parameters in hippocampal extracts from p21 C57 *Fmr1 KO* mice, a developmental time point at which these mice exhibit an accepted seizure phenotype (Fig. 1). Immunoblotting revealed that phosphorylation of S443 in the α4 subunit was significantly decreased in *Fmr1 KO* mice 80 ± 9%% of control (n=4 for WT and *Fmr1 KO* p=0.001), while that for total α4 subunit levels and β3 S408/9 was increased 118 ± 4% of control, and 120 ± 6% of control respectively (n=6 for WT and *Fmr1 KO*; p=0.005). In contrast, phosphorylation of β3 S383 was comparable between genotypes. Interestingly, total α2 was decreased to 91 ± 5 % of WT (n=5 WT, n=4 *Fmr1 KO*; P = 0.04). In contrast to this, the total expression levels of α1, α5, β3, δ and γ2 subunits were comparable between genotypes. Finally, we examined if these changes in $GABA_A$R expression level and phosphorylation persist in adult mice. Significantly, in p48-72 C57 *Fmr1 KO* mice did not exhibit any deficits in

$GABA_AR$ expression levels or phosphorylation (Fig. 1B). This experiment demonstrates that there are alterations in the phosphorylation and expression levels of $GABA_ARs$ in *Fmr1 KO* mice.

Synaptic targeting of α4 subunit containing $GABA_ARs$ in *Fmr1 KO* mice. Because changes in subunit phosphorylation can affect the trafficking of $GABA_ARs$ in the membrane we examined the cellular distribution of the α4 subunit. We stained 40 μm hippocampal slices with antibodies against the α4 subunit together with antibodies against the inhibitory postsynaptic inhibitory protein gephyrin. Using confocal microscopy coupled with *Metamorph* analysis we examined the α4 subunit/gephyrin positive puncta in the dentate gyrus between genotypes.

As illustrated in Fig. 2, there appeared to be an increase in α4 subunit immunoreactivity at gephyrin positive structures in the brains of *Fmr1 KO* mice suggesting an abnormal redistribution of extrasynaptic α4 subunit to synaptic locations.

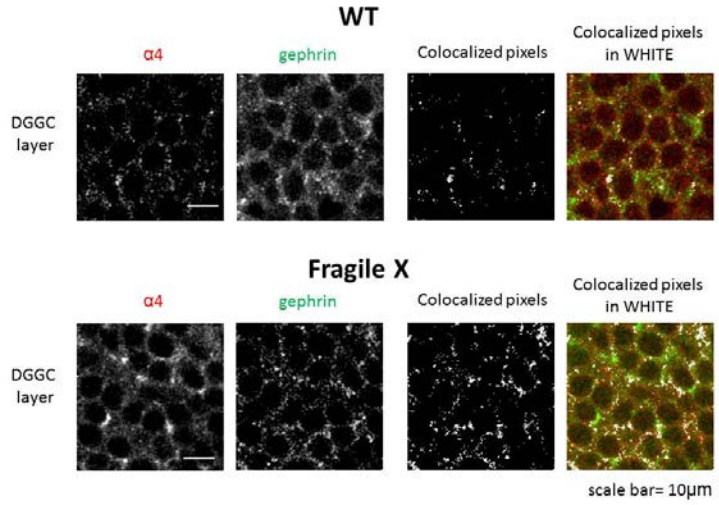

Figure 2. Characterization of α4-containing inhibitory synapses in Fmr1 KO. *40μm hippocampal slices were stained with antibodies against the $GABA_AR$ α4 subunit and gephyrin, a marker of inhibitory synapses. The number of α4/gephyrin positive puncta was compared within the dentate gyrus between genotypes. In Fmr1 KO mice, the number of α4 colocalized with gephyrin increased, consistent with an increase in the altered localization of α4-containing $GABA_ARs$ to inhibitory synapses.*

NASs increase the phosphorylation and cell surface stability of $GABA_ARs$.

We have previously shown that the naturally occurring NAS, THDOC, increased tonic current in part through phosphorylation of S408/409 of the β3 subunit (Abramian et al., 2014; Vien et al., 2015). The

temporal effects of THDOC on $GABA_AR$ phosphorylation were examined in hippocampal slices. S443 phosphorylation was significantly enhanced at 5 min, but returned to basal levels by 20 min. S408/9 phosphorylation did not reach statistical significance until 10 min, but was maintained at 20 min. NS dependent $GABA_AR$ phosphorylation was blocked by GFX (Fig. 3A).

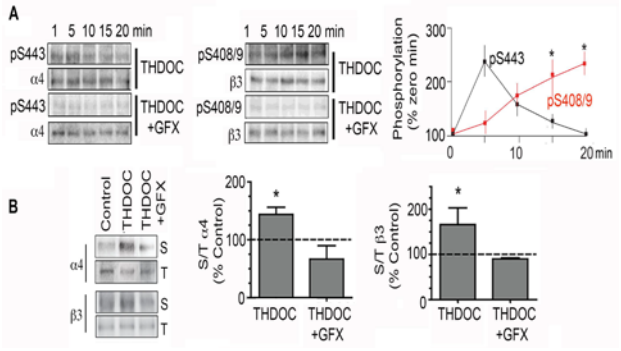

Figure 3. NASs potentiate phosphorylation and cell surface stability of $GABA_AR$. A. *Hippocampal slices were treated with, 100 nM THDOC, or 100 nM THDOC with 50 μM GFX for 20 min. SDS soluble lysates were then immunoblotted with pS443, pS408/9, α4 and β3 subunit antibodies. The ratio of pS443/α4 and pS408/9/β3 immunoreactivity were then determined and normalized to values seen at zero time (100%).* ***B****. Slices were labeled with Sulfo-NHS-SS-biotin. After lysis and purification on avidin, surface and total fractions were immunoblotted with α4 and β3 subunit antibodies. The ratio of surface:total immunoreactivity (S/T) for each subunit were then normalized to vehicle treated controls (100%; dotted line). * = significantly different to control* $p<0.05$ (t-test, n= 6 mice)**.**

In parallel with potentiating phosphorylation, THDOC increased the cell surface expression levels of both subunits, dependent upon PKC activity (Fig. 3B). Thus, our results suggest that NASs enhance the phosphorylation and cell surface accumulation of $GABA_AR$ containing α4 and β3 subunits.

To further our understanding of the NAS-mediated increase in tonic current we measured the effects of ALLO, and SGE-516 on the phosphorylation and membrane expression of β3 subunits in hippocampal slices. Twenty min exposure to 100nM ALLO, or SGE-516 increased phosphorylation of β3 subunits at S408/409 to 141 ± 10% of control ($n=10$, $p<0.01$), and 143 ± 14% of control ($n=4$, $p<0.05$) respectively (Fig. 4A&B).

Figure 4. NAS exposure increases phosphorylation and surface expression of β3 subunits. A. *Exposure to 100 nM of the NASs, ALLO or SGE-516, for 20 min increases β3 S408/409 phosphorylation in acute hippocampal slices.* ***B.*** *The ratio of p-β3/T-β3 was measured and values were normalized to those in control (100%). Asterisks represent a significant difference from control (ALLO: p <0.01, Student's t test, n=10; SGE-516: p<0.05, Student's t test, n=4).* ***C.*** *Exposure to 100 nM ALLO or SGE-516 for 20 min increases $GABA_A$-β3–containing receptors at the plasma membrane in acute hippocampal slices.* ***D.*** *The ratio of surface β3/T-β3 was measured and values were normalized to cell surface levels in control treated slices (100%). Asterisks represent a significant difference from control (ALLO: p <0.05, Student's t test, n=8; SGE-516: p<0.05, Student's t test, n=4).*

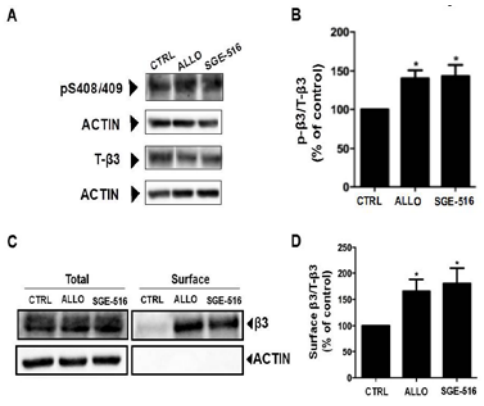

In parallel with modulating phosphorylation, exposure to 100 nM ALLO, or SGE-516 increased the cell surface expression levels of receptors containing β3 subunits to 166 ± 22% of control (n=8, p<0.05), and 180 ± 29% of control (n=4, p<0.05) respectively (Fig. 4C&D). Therefore, in parallel with inducing sustained effects on GABAergic inhibition ALLO and SGE-516 enhance the cell surface levels and phosphorylation of the $GABA_A$Rs containing β3 subunits dependent upon PKC activity.

Specific Aim 2. Determining exposure to neurosteroids enhances the efficacy of tonic inhibition in FXS. (PI: Davies)

Neuroactive steroids reverse the deficits in tonic inhibition. We analyzed the sustained effects of ALLO, or the new synthetic NAS SGE-516 on the tonic current in DGGCs in hippocampal slices from 3-5 week old C57 male mice. Hippocampal slices were incubated for 15 min in a chamber containing NASs dissolved in ACSF. Slices were then transferred to the recording chamber of the microscope followed by a wash period between 30 to 60 mins of continuous perfusion of NAS-free ACSF before recordings were started (Fig. 5A).

Slices exposed to ALLO, or SGE-516 demonstrated a concentration-dependent increase in the tonic current measured by the addition of picrotoxin with the maximal effects at 1 μM. Control, vehicle-

treated slices had a tonic current of 43.6 ± 5.7 pA (n=12), whereas the tonic currents for slices treated with SGE-516 (1 μM) was 123.0 ± 22.2 pA, (n=6, p= 0.0003), or ALLO (1 μM) was 95.8 ± 10.8 pA (n=4, p= 0.0005, Fig. 5B&C).

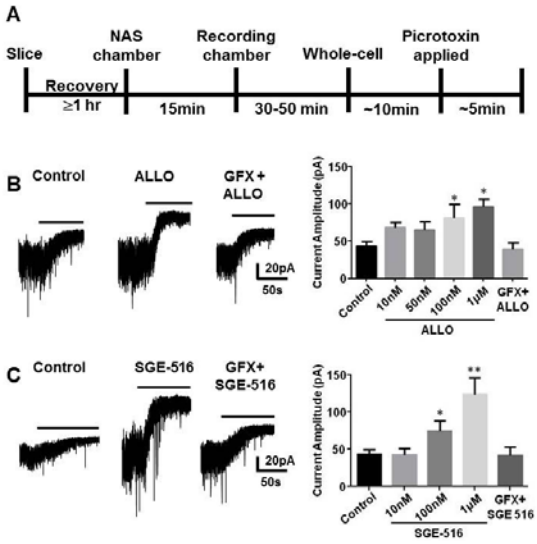

Figure 5. NAS-mediated metabotropic enhancement of tonic inhibitory current in DGGC neurons. A. *Scheme demonstrating experimental protocol. Hippocampal slices were allowed to recover for at least 1 hr following slicing. Slices were then incubated for 15 min in a chamber containing NASs dissolved in ACSF. Slices were then transferred to the recording chamber of the microscope followed by a wash period between 30 to 60 min of continuous perfusion of NAS-free ACSF before recordings were started. Recordings were made from DGGCS in hippocampal slices from p21-35 C57 mice in the presence of 1 μM GABA followed by 100 μM picrotoxin and the difference in holding current was then determined.* ***Left panel B & C.*** *Example tonic currents from slices following exposures to vehicle (control) or 100 nM ALLO (B), 100 nM SGE-516 (C) for 15 min. No change in tonic current was observed in slices pre-incubated for 15 min with GFX followed by ALLO, or SGE-516. Bar above current represents application of picrotoxin (100μM).* ***Right panel B & C.*** *Bar graph shows average tonic current was significantly enhanced following exposure to different concentrations of ALLO and SGE-516. In all panels * = significantly different to control (p<0.05; t-test, n=4-12 cells).*

Synaptic targeting of α4 subunit containing $GABA_A$Rs in Fmr1 KO mice. We have previously noted that IPSC biophysical properties changed in the *Fmr1 KO* mouse, with the IPSC amplitude increasing and the decay prolonging compared to wild-type. The data presented above shows an increase in α4 subunit immunoreactivity at gephyrin positive structures in the hippocampus suggesting the α4 subunit at synapses. We have assessed the effects of the benzodiazepine diazepam (which enhance αβγ2 $GABA_A$Rs where α can be 1-3 subunits) on sIPSC amplitude, and decay in WT and *Fmr1 KO* mice. Additionally, we have examined the α4βγ2 specific benzodiazepine Ro15-4513 on sIPSC properties between genotypes.

In wild type mice, diazepam significantly enhanced IPSC amplitude and prolonged decay whereas in *Fmr1 KO* mice only decay was prolonged (Fig 6A&B). Conversely, in the presence of Ro15-4513, IPSC amplitude and decay where unchanged in wild type mice but were significantly enhanced in the *Fmr1 KO* mice (Fig 6C&D).

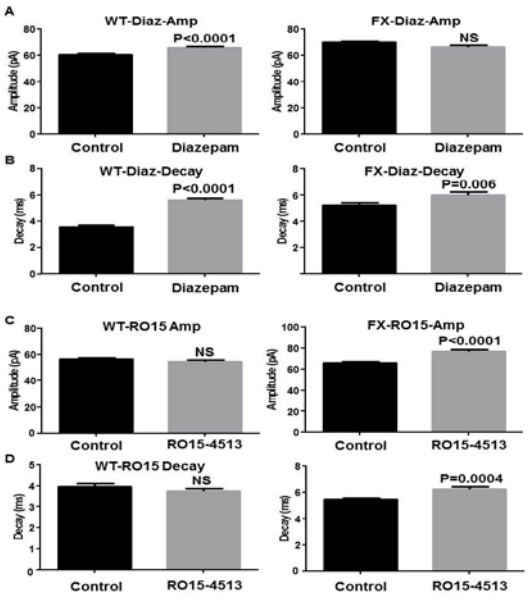

Figure 6. Modulation of DGGC IPSCs by benzodiazepines. *Recordings were made from DGGCs in hippocampal slices from p21-35 WT, or Fmr1 KO mice. Fmr1 KO mice displayed larger sIPSC amplitudes and longer decay times compared to age-matched controls.* Bar graphs show the effects of acute (10min) exposures to diazepam (A&B) or Ro15-4513 (C&D) applied to slices from wild-type (left column) and Fmr1 KO (right column) mice.

These data suggest the involvement of α4 subunit in synaptic $GABA_A$Rs. This is a new finding in the FXS field and could explain the poor clinical effects of benzodiazepines because α4 subunits are insensitive to the modulation by most benzodiazepines.

The impact of modified GABAergic inhibition on circuit excitability in Fmr1 KO mice. We have examined the circuit excitability of the hippocampus using a perforated multi-electrode array (pMEA) system. A deficit in tonic current observed in *Fmr1 KO* mice is hypothesized to reduce tonic inhibition which would increase the overall circuit excitability by increasing the likelihood of neurons to fire action potentials. It has been proposed that in FXS there is an increase in neuronal excitability and synchrony across various brain structures (Goncalves et al 2013). Our preliminary data demonstrating a reversal of the tonic current deficit in *Fmr1 KO* with NS treatment would be expected to restore tonic inhibition and reduce the excessive circuit excitability.

Seizure-like events (Padgett et al) were induced by low Mg^{2+} artificial cerebrospinal fluid (ACSF) to relieve the Mg^{2+} block of NMDA receptors (Traub et al 1994). We obtained preliminary data with a

pMEA on loan from the supplier. We recorded field potentials from horizontal cortical-hippocampal slices from WT and *Fmr1 KO* mice (Fig.7B).

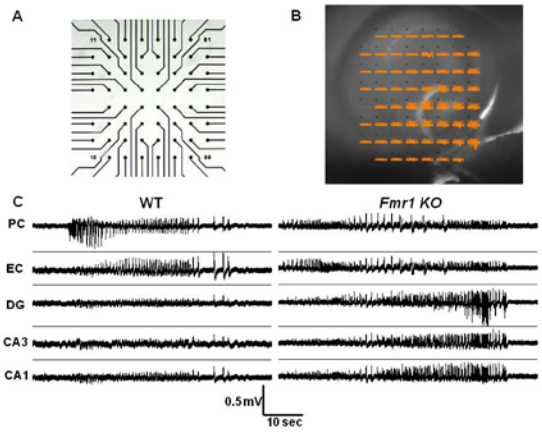

Figure 7. In vitro seizure like events (SLE) in hippocampal slices from WT and Fmr1 KO mice in the absence of Mg^{+2} using multi-electrode array (MEA) system. *Hippocampal slices from Fmr1 KO and WT mice were tested for seizure like events (SLE) in absence of Mg^{+2} using MEA.* ***A.*** *Multi-electrode array chamber* ***B.*** *MEA-layout (iii). Typical slice on MEA-layout (iv) MEA stage & amplifier.* ***C.*** *Traces showing the first SLEs from the dentate gyrus (DG), CA3 neurons (CA3), CA1 neurons (CA1), entorhinal cortex (EC), postrhinal cortex (PC) regions of the hippocampal slices from WT and Fmr1 KO mice.*

SLEs were induced by perfusing the recording chamber with low Mg^{2+} ACSF. SLEs were characterized by tonic-clonic discharges, with an initial tonic phase followed by a period of clonic after-discharges. Interestingly, we observed a dramatic regional difference in SLE propagation (Fig. 7C). In the WT slices, the first SLE occurred in the entorhinal cortex (EC) and postrhinal cortex (PC) but did not show full propagation through the dentate gyrus (DG). In contrast, the first SLEs in *Fmr1 KO* slices propagated through the DG, indicating an increased potential susceptibility of DG recruitment during onset of epileptiform activity in slices from *Fmr1 KO* mice. The DG is known to be important for epileptogenesis because it forms the so-called dentate-gate that prevents activity spreading from cortex to the hippocampus. Tonic inhibition in the dentate gyrus seems to be critical in preventing excessive neuronal excitability.

Increased excitability of granule cells in *Fmr1 KO* mice. Neuronal excitability is greatly influenced by tonic inhibition. Because of the decrease in DGGC tonic inhibition observed in *Fmr1 KO* mice we next examined input-output curves on DGGCs to measure the intrinsic excitability of the neurons. We delivered current step injections to depolarize the membrane and measured the action potentials elicited from those current injections. There was a clear increase in action potential firing rate at lower current injections in DGGCs from *Fmr1 KO* mice compared to WT DGGCs, with a leftward shift in the relationship between firing rate and injected current (Fig 8).

The ability of NASs to reverse the deficit in tonic current would suggest that NAS exposure could reduce neuronal excitability. Hippocampal slices were exposed to SGE-516 for 15 min followed by a >30 min washout period before the input-output relationship was examined. SGE-516 exposure reduced membrane excitability of DGGCs from *Fmr1 KO* mice, causing a rightward shift in the input-output curve similar to that of vehicle treated WT DGGCs.

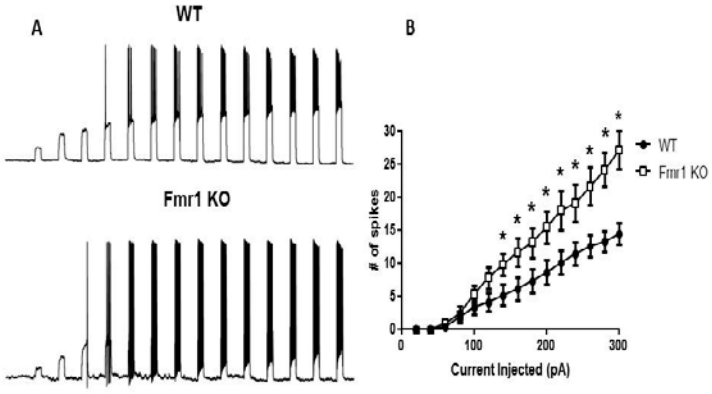

Figure 8. DGGCs from Fmr1 KO mice are more excitable than from WT mice. A. *Representative recordings of action potential firing in DGGCs from WT and Fmr1 KO mice in response to 0.5s current injections from 20 to 300 pA in 20 pA increments.* ***B.*** *Average input/output curves representing the average number of action potentials from WT (black circles) and Fmr1 KO mice (open boxes). Values are means ± SE; n = 2 mice, 6 cells per experimental group. *P < 0.05 denotes statistical significance compared with WT littermates using Student's t-test.*

Specific Aim 3. Ascertaining behavioral phenotypes in Fmr1 KO mice will be reversed with NS exposure. (PI: Davies).

Recently, a publication from Sage Therapeutics demonstrated the effectiveness of SGE-516 in protecting *Fmr1 KO* mice against audiogenic seizures (Hammond et al., 2017). Rather than repeat these experiments we examined the EEG activity in *Fmr1 KO*. There are very few published reports on EEG activity from these mice which could provide valuable data on behavior based on electrical activity. In human FXS patients abnormal EEG data in childhood has been suggested as a predictor of anxiety in later life (Sinclair et al., 2017).

Examine the effects of NAS exposure on electroencephalogram activity of *Fmr1 KO* mice. FXS patients have sleep disturbances and seizures in these patients occur more frequently during sleep

(Musumeci et al 1990, Musumeci et al 1999). In the *Fmr1 KO* mouse model of FXS it has been shown that there are abnormal neuronal firing rates, particularly during sleep (Goncalves et al 2013, Pavlov et al 2009). Electroencephalogram (EEG), and electromyogram (EMG) electrodes were inserted into mice anesthetized with isoflurane. Following acclimation, EEG/EMG activity was continuously monitored for 3 hours.

Preliminary studies demonstrated that EEG activity across all frequencies was increased in *Fmr1 KO* mice compared to WT (Fig. 9). Administration of a single injection of SGE-516 (3 mg/kg i.p.) increased θ and γ activity in WT but decreased the δ activity in *Fmr1 KO* mice.

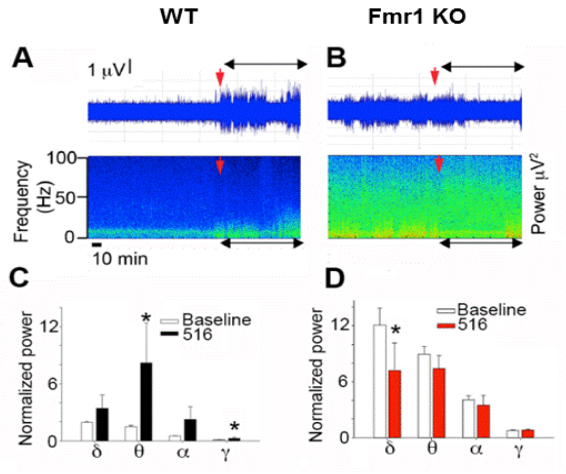

Figure 9. Effects of SGE-516 injection on EEG recordings from WT and Fmr1 KO mice EEG recording and corresponding spectrogram for a single WT mouse (**A**) and *Fmr1 KO* mouse (**B**). SGE-516 (3mg/Kg i.p.) was injected at 80 min (red arrow). **C&D.** Cumulative average of specific bands for WT and *Fmr1 KO* mice respectively (n=4). Scales are normalized power (μv^2) for 1 hr before injection and 1 hr after. A 2-way ANOVA was used to calculate significance * $p<0.05$. All recordings were performed at 1000Hz using a Pinnacle headmount preamplifier.

The synchronized cortical activity has been explained by an increase in neuronal firing rates and predisposes the animal to seizures, hyperactivity, and a reduced computational ability of the cerebral cortex (Goncalves et al 2013). We believe NAS treatment will normalize EEG activity due to the increased tonic inhibition preventing the increase in neuronal firing.

What opportunities for training and professional development has the project provided?

Dr. Amit Modgil participates in lab meetings, presenting data on a regular basis. Amit will also present his findings to the whole Neuroscience Department once a year in our post-doctoral research seminar

series. He also attends weekly department seminars. In addition the postdoctoral program at Tufts runs a weekly career development seminar series. Speakers in this series are drawn from the local pharmaceutical and biotechnology industry in the local area, which highlights the range of career opportunities for life scientist with doctoral degrees. He also attends didactic and tutorial courses related to animal care and use, laboratory safety, radiation safety and the responsible conduct of research.

Dr Amit Modgil was selected to give an oral presentation at the Gordan Research Seminar for "Fragile X and Autism-Related Disorders". Dr Modgil also presented a poster at the Gordan Research Conference for "Fragile X and Autism-Related Disorders" in Vermont, June 2016.

How were the results disseminated to communities of interest?

Dr Modgil and Dr Davies presented a poster at the "Neuro Developmental Disorders symposium" at Harvard Medical School, October 2015.

Dr Amit Modgil gave an oral presentation at Gordan Research Seminar for "Fragile X and Autism-Related Disorders". Dr Modgil and Dr Davies presented posters at the Gordan Research Conference for "Fragile X and Autism-Related Disorders" in Vermont, June 2016.

Findings from the study are being submitted as a manuscript.

What do you plan to do during the next reporting period to accomplish the goals?

Nothing to Report

4. Impact

What was the impact on the development of the specific discipline(s) of the project?

The α4 subunits are usually thought to be located extrasynaptically mediating tonic inhibition. In FXS it is believed that the expression of α4 subunit containing $GABA_A$Rs is reduced, thereby decreasing the

contribution of tonic inhibition to the overall inhibition in neurons resulting in excessive excitation. However, our data has suggested that the change in phosphorylation of subunits in *Fmr1 KO* mice leads to a redistribution of subunits which cause a reduction of tonic current and an alteration of phasic inhibition. The relocation of the α4 subunit, in particular, to synaptic sites not only alters phasic current biophysics it also changes the pharmacological response to benzodiazepines. This has not been observed before in FXS models and can help explain the lack of benzodiazepine efficacy in FXS. Our data also point to tonic inhibition contributing significantly to the "dentate gate", an important characteristic of the dentate gyrus in limiting excessive neuronal activity flowing into the hippocampus and out back into the cortex.

What was the impact on other disciplines?

The breakdown of the dentate gate because of the redistribution of the α4 subunit and reduction of tonic current will impact the knowledge in the epilepsy field. Neuroactive steroids are known to have many impacts on health, including anxiety, depression, and neurogenesis.

What was the impact on technology transfer?

This project could impact the therapeutic targets used by pharmaceutical companies. Most GABAergic compounds to date have been developed as positive allosteric modulators. However, this project indicates that mechanisms which influence trafficking of subunits would be a valid therapeutic target.

What was the impact on society beyond science and technology?

Nothing to report.

5. Changes/Problems

Nothing to Report

6. Products

Publications resulting from the work under this award:

Vien TN, Modgil A, Abramian AM, Jurd R, Walker J, Brandon NJ, Terunuma M, Rudolph U, Maguire J, **Davies PA**, Moss SJ (2015). Compromising the phosphodependent regulation of the GABAAR β3 subunit reproduces the core phenotypes of autism spectrum disorders. Proc Natl Acad Sci U S A., 112:14805-14810. Published; acknowledged federal support.

Modgil A, Parakala ML, Ackley MA, James J. Doherty JJ, Stephen J. Moss SJ, **Davies PA** (2017). Endogenous and synthetic neuroactive steroids evoke sustained increases in the efficacy of GABAergic inhibition via a protein kinase C-dependent mechanism. *Neuropharmacology*, **113**:314-322.; acknowledged federal support.

Other publications during reporting period:

Kelley MR, Deeb TZ, Brandon NJ, Dunlop J, **Davies PA**, Moss SJ (2016). Compromising KCC2 transporter activity enhances the development of continuous seizure activity. *Neuropharmacology*, **108**:103-110.

Nakamura Y, Morrow DH, Modgil A, Huyghe D, Deeb TZ, Lumb MJ, **Davies PA**, Moss SJ. Proteomic Characterization of Inhibitory Synapses Using a Novel pHluorin-tagged γ-Aminobutyric Acid Receptor, Type A (GABAA), α2 Subunit Knock-in Mouse. J Biol Chem. 2016;291:12394-407. Published; acknowledged federal support.

7. Participants & Other Collaborating Organizations

What individuals have worked on the project?

Name: Paul A. Davies

Project Role: co-PI, Initiating PI

Researcher Identification (ORCID ID): 0000-0002-3973-3143

Nearest person month worked: 3 calendar months

Contribution to Project: Has designed experiments and performs analysis and interpretation of the results. He also supervises other members of the research team and is responsible for writing reports and producing manuscripts.

Funding Support: NIH-NIMH R01 MH097446

Name: Stephen J. Moss

Project Role: co-PI

Researcher Identification:

Nearest person month worked: 0.5 calendar months

Contribution to Project: Supervising the experiments designed to assay the effects of neurosteroids on $GABA_AR$ phosphorylation and cell surface accumulation.

Funding Support: NIH-NIDA DA037170-01, NIH-NIMH R01 MH097446, NIH-NINDS R01 NS081986, NIH-NINDS, 1R01NS087662, AstraZeneca; IMED/$GABA_BR$ drug development.

Name: Amit Modgil

Project Role: Postdoctoral Researcher

Researcher Identification:

Nearest person month worked: 6 calendar months

Contribution to Project: Has performed the electrophysiology experiments, making hippocampal slices and examining the effects of their exposure to neurosteroids.

Funding Support: Funded from R01 MH097446

Name: Manasa L. Parakala

Project Role: Graduate student

Researcher Identification:

Nearest person month worked: 6 calendar months

Contribution to Project: Has performed the biochemistry experiments examining $GABA_AR$ phosphorylation and cell surface accumulation.

Funding Support: Funded from R01 MH097446

Has there been a change in the active other support of the PD/PI(s) or senior/key personnel since the last reporting period?

Nothing to report

What other organizations were involved as partners?

Organization Name: SAGE Therapeutics

Location of Organization: Cambridge, MA

Partner's contribution to the project:

Collaboration. SAGE Therapeutics share the necessary proprietary compounds and data necessary to support the success of this project

8. Special Reporting Requirements

Collaborative Award

9. Appendices

Vien TN, Modgil A, Abramian AM, Jurd R, Walker J, Brandon NJ, Terunuma M, Rudolph U, Maguire J, Davies PA, Moss SJ. Compromising the phosphodependent regulation of the GABAAR β3 subunit reproduces the core phenotypes of autism spectrum disorders. Proc Natl Acad Sci U S A. 2015;112:14805-14810.

Modgil A, Parakala ML, Ackley MA, James J. Doherty JJ, Stephen J. Moss SJ, Davies PA (2017). Endogenous and synthetic neuroactive steroids evoke sustained increases in the efficacy of GABAergic inhibition via a protein kinase C-dependent mechanism. Neuropharmacology, 113:314-322.

Neuropharmacology 113 (2017) 314–322

Contents lists available at ScienceDirect

Neuropharmacology

journal homepage: www.elsevier.com/locate/neuropharm

Endogenous and synthetic neuroactive steroids evoke sustained increases in the efficacy of GABAergic inhibition via a protein kinase C-dependent mechanism

Amit Modgil [a], Manasa L. Parakala [a], Michael A. Ackley [b], James J. Doherty [b], Stephen J. Moss [a, c], Paul A. Davies [a, *]

[a] Tufts University School of Medicine, Department of Neuroscience, 136 Harrison Ave, Boston, MA 02111, USA
[b] Sage Therapeutics, Inc., 215 First St, Cambridge, MA, USA
[c] Department of Neuroscience, Physiology and Pharmacology, University College, London WC1E6BT, United Kingdom

ARTICLE INFO

Article history:
Received 10 May 2016
Received in revised form
3 October 2016
Accepted 9 October 2016
Available online 12 October 2016

Keywords:
GABA receptor
Protein kinase C (PKC)
Neuroactive steroid
Tonic inhibition
Dentate gyrus

ABSTRACT

The neuroactive steroid (NAS) tetrahydrodeoxycorticosterone (THDOC) increases protein kinase C (PKC) mediated phosphorylation of extrasynaptic $GABA_A$ receptor ($GABA_AR$) subunits leading to increased surface expression of α4/β3 subunit-containing extrasynaptic $GABA_ARs$, leading to a sustained increase in $GABA_AR$ tonic current density. Whether other naturally occurring and synthetic NASs share both an allosteric and metabotropic action on $GABA_ARs$ is unknown. Here, we examine the allosteric and metabotropic properties of allopregnanolone (ALLO), and synthetic NASs SGE-516 and ganaxolone. ALLO, SGE-516, and ganaxolone all allosterically enhanced prototypical synaptic and extrasynaptic recombinant $GABA_ARs$. In dentate gyrus granule cells (DGGCs) all three NASs, when applied acutely, allosterically enhanced tonic and phasic GABAergic currents. In separate experiments, slices were exposed to NASs for 15 min, and then transferred to a steroid naïve recording chamber followed by ≥ 30 min wash before tonic currents were measured. A sustained increase in tonic current was observed following exposure to ALLO, or SGE-516 and was prevented by inhibiting PKC with GF 109203X. No increase in tonic current was observed with exposure to ganaxolone. In agreement with the observations of an increased tonic current, the NASs ALLO and SGE-516 increased the phosphorylation and surface expression of the β3 subunit-containing $GABA_ARs$. Our studies demonstrate that neuroactive steroids have differential abilities to induce sustained increases in the efficacy of tonic inhibition by promoting $GABA_AR$ phosphorylation and membrane trafficking dependent on PKC activity.

1. Introduction

γ-Aminobutyric acid type A receptors ($GABA_ARs$) mediate both phasic and tonic inhibitory neurotransmission in the CNS and are the sites of action of benzodiazepines, barbiturates, general anesthetics and neuroactive steroids (NAS). $GABA_ARs$ containing the α4 subunit are located primarily extrasynaptically in the dentate gyrus of the hippocampus, neocortex, striatum and the thalamus where they are persistently activated by low concentrations of GABA. They have distinct pharmacological properties that distinguish them from synaptic $GABA_ARs$ (Glykys and Mody, 2007). Extrasynaptic $GABA_ARs$ are responsible for mediating the tonic inhibition that determines the gain and offset of the neuronal output, thus regulating the excitability of neurons and the activity of neuronal circuits (Belelli et al., 2009; Semyanov et al., 2004). In addition to regulating neuronal activity, α4/δ subunit-containing $GABA_ARs$ are implicated in a multitude of neurological disorders including epilepsy, neurodevelopment disorders and anxiety disorders (Belelli et al., 2009; Brickley and Mody, 2012; D'Hulst and Kooy, 2007).

The endogenous NASs ALLO, and THDOC, and the synthetic NAS ganaxolone, are potent positive allosteric modulators (PAMs) of $GABA_ARs$. Consistent with their role as $GABA_AR$ PAMs, NASs have dose dependent anxiolytic, anti-convulsant, hypnotic and sedative actions (Mitchell et al., 2008; Paul and Purdy, 1992). The ability of NASs to allosterically potentiate both phasic and tonic inhibition makes them attractive anticonvulsants however, despite these

* Corresponding author.
E-mail address: paul.davies@tufts.edu (P.A. Davies).

http://dx.doi.org/10.1016/j.neuropharm.2016.10.010
0028-3908/

favorable properties the therapeutic potential of NASs is very limited because of their low bioavailability, and rapid clearance preventing the concentration in the brain to reach therapeutic levels (Rupprecht, 2014). Recently, Botella et al (Botella et al., 2015). developed a series of synthetic NASs with modification that highly improves their pharmacokinetic properties yet retain similar pharmacological profile as ALLO. Among those compounds, SGE-516 was developed with improved bioavailability, and pharmacokinetic properties.

In addition to their actions as PAMs, recent studies have demonstrated that THDOC has a metabotropic mechanism of action on $GABA_A$Rs. THDOC increase the PKC-dependent phosphorylation of S443 in α4 subunits and S408/9 in β3 subunits. Upon THDOC exposure, enhanced phosphorylation at S443 and S408/9 leads to a sustained increase in $GABA_A$R tonic current density due to increased receptor insertion into the plasma membrane and decreased receptor endocytosis (Abramian et al., 2010, 2014; Adams et al., 2015). In this study we sought to examine if the PKC-dependent metabotropic pathway previously identified with THDOC exposure is stimulated by another endogenous NAS, ALLO, the first generation synthetic NAS, ganaxolone, and a more recently developed synthetic NAS, SGE-516.

2. Methods

2.1. Recombinant $GABA_A$ pharmacology

Cellular electrophysiology was used to measure the pharmacological properties of ALLO, ganaxolone and SGE-516 in heterologous cell systems. Compounds were tested for their ability to affect GABA mediated currents at a submaximal agonist dose (GABA $EC_{20} = 2$ μM).

LTK cells were stably transfected with the α1β2γ2 subunits of the GABA receptor and CHO cells are transiently transfected with the α4β3δ subunits via the Lipofecatamine method. Cells were passaged at a confluence of about 50–80% and then seeded onto 35 mm sterile culture dishes containing 2 ml culture complete medium without antibiotics or antimycotics. Cells were cultivated at a density that enabled the recording of single cells without visible connections to other cells.

Whole-cell currents were measured with HEKA EPC-10 amplifiers using PatchMaster software. Bath solution for all experiments contained (in mM): NaCl 137, KCl 4, $CaCl_2$ 1.8, $MgCl_2$ 1, HEPES 10, D-Glucose 10, pH 7.4 with NaOH. Intracellular (pipette) solution contained (in mM): KCl 130, $MgCl_2$ 1, Mg-ATP 5, HEPES 10, EGTA 5, pH 7.2 with KOH. During experiments, cells and solutions were maintained at room temperature (19 °C - 30 °C). For manual patch-clamp recordings, cell culture dishes were placed on the dish holder of the microscope and continuously perfused (1 ml/min) with bath solution. After formation of a Gigaohm seal between the patch electrode and the cell (pipette resistance range: 2.5 MΩ - 6.0 MΩ; seal resistance range: >1 GΩ) the cell membrane across the pipette tip was ruptured to assure electrical access to the cell interior (whole-cell patch configuration).

Cells were voltage-clamped at a holding potential of −80 mV. $GABA_A$ receptors were activated by 2 μM GABA and compounds were sequentially applied at increasing concentrations for 30s prior to a 2s application of GABA. GABA and compounds were applied to cells via the Dynaflow perfusion system (Cellectricon, Sweden). Test compounds were dissolved in DMSO to form 10 mM stock solution and serially diluted to 0.01, 0.1, 1, and 10 μM in bath solution. There was no effect on GABA currents when DMSO was applied to cells at its maximal concentration in solution (0.1%). All concentrations of test compound were tested on each cell. The relative percentage potentiation was defined as the peak amplitude in response to GABA EC_{20} in the presence of test compound divided by the peak amplitude in response to GABA EC_{20} alone, multiplied by 100.

2.2. Hippocampal slice preparation

Brain slices were prepared from 3- to 5-week-old male C57 mice. Mice were anesthetized with isoflurane, decapitated, and brains were rapidly removed and submerged in ice-cold cutting solution containing (mM): 126 NaCl, 2.5 KCl, 0.5 $CaCl_2$, 2 $MgCl_2$, 26 $NaHCO_3$, 1.25 NaH_2PO_4, 10 glucose, 1.5 sodium pyruvate, and 3 kynurenic acid. Coronal 310 μm thick slices were cut with the vibratome VT1000S (Leica Microsystems, St Louis, MO, USA). The slices were then transferred into incubation chamber filled with prewarmed (31–32 °C) oxygenated artificial cerebro-spinal fluid (ACSF) of the following composition (in mM): 126 NaCl, 2.5 KCl, 2 $CaCl_2$, 2 $MgCl_2$, 26 $NaHCO_3$, 1.25 NaH_2PO_4, 10 glucose, 1.5 sodium pyruvate, 1 glutamine, 3 kynurenic acid and 0.005 GABA bubbled with 95% O_2 −5% CO_2. Slices were allowed to recover at 32 °C for at least 1hr before recording. Exogenous GABA was added in an attempt to standardize ambient GABA in the slice and provide an agonist source for newly inserted extrasynaptic $GABA_A$Rs.

2.3. Electrophysiology recordings

After recovery, a single slice was transferred to a submerged, dual perfusion recording chamber (Warner Instruments, Hamden, CT, USA) on the stage of an upright microscope (Nikon FN-1) with a 40× water immersion objective equipped with DIC/IR optics. Slices were maintained at 32 °C and gravity-superfused with ACSF solution throughout experimentation and perfused at rate of 2 ml/min with oxygenated (O_2/CO_2 95/5%) ACSF.

Whole-cell currents were recorded from the dentate gyrus granule cells (DGGCs) in 310-μm-thick coronal hippocampal slices. Patch pipettes (5–7 MΩ) were pulled from borosilicate glass (World Precision Instruments) and filled with intracellular solution of the composition (in mM) as follows: 140 CsCl, 1 $MgCl_2$, 0.1 EGTA, 10 HEPES, 2 Mg-ATP, 4 NaCl and 0.3 Na-GTP (pH = 7.2 with CsOH). A 5 min period for stabilization after obtaining the whole-cell recording conformation (holding potential of −60 mV) was allowed before currents were recorded using an Axopatch 200B amplifier (Molecular Devices), low-pass filtered at 2 kHz, digitized at 20 kHz (Digidata 1440A; Molecular Devices), and stored for off-line analysis.

2.4. Electrophysiology analysis

For tonic current measurements, an all-points histogram was plotted for a 10 s period before and during 100 μM picrotoxin application, once the response reached a plateau level. Recordings with unstable baselines were discarded. Fitting the histogram with a Gaussian distribution gave the mean baseline current amplitude and the difference between the amplitudes before and during picrotoxin was considered to be the tonic current. The negative section of the all-points histogram which corresponds to the inward IPSCs was not fitted with a Gaussian distribution (Kretschmannova et al., 2013; Nusser and Mody, 2002). Series resistance and whole-cell capacitance were continually monitored and compensated throughout the course of the experiment. Recordings were eliminated from data analysis if series resistance increased by >20%.

Spontaneous inhibitory post-synaptic currents (sIPSCs) were analyzed using the mini-analysis software (version 5.6.4; Synaptosoft, Decatur, GA). Minimum threshold detection was set to 3 times the value of baseline noise signal. To assess sIPSC kinetics, the

recording trace was visually inspected and only events with a stable baseline, sharp rising phase, and single peak were used to negate artifacts due to event summation. Only recordings with a minimum of 200 events fitting these criteria were analyzed. sIPSCs amplitude, and frequency from each experimental condition was pooled and expressed as mean ± SEM. To measure sIPSC decay we averaged 100 consecutive events and fitted the decay to a double exponential and took the weighted decay constant (τ_w). Statistical analysis was performed by using Student t-test (paired and unpaired where appropriate), where $p < 0.05$ is considered significant.

2.5. Metabolic labeling and biotinylation

Hippocampi were dissected out of acute slices from 8 to 12 week old C57/Bl6 mice and lysed with phosphate buffer including: 20 mM Tris-HCl, 150 mM NaCl, 5 mM EDTA, 10 mM NaF, 2 mM Na3VO4, 10 mM pyrophosphate, 0.1% SDS and 1% Triton after drug treatment. The β3 subunit was isolated using immunoprecipitation with β3 antibodies, after correction for protein content and the specific activity of labeling. Results were attained by SDS/PAGE followed by autoradiography (Abramian et al., 2010). For biotinylation experiments hippocampi were dissected out of acute slices from 8 to 12 week old C57/Bl6 mice and incubated in artificial cerebrospinal fluid (ACSF) described above at 30 °C for 1 h for recovery before experimentation. Slices were then placed on ice and incubated for 30 min with 1 mg/mL NHS-SS-biotin (Pierce). Excess biotin was removed by a 50 mM glycine quenching buffer, followed by washing of slices three times in ice-cold ACSF. The tissue was snap frozen on dry ice for 5 min, thawed at 4 °C and lysed. The lysates were solubilized with 2% Triton at 4 °C on a rotating wheel for 1 h. The insoluble material was removed by centrifugation, and 350–500 μg of protein lysate were incubated with NeutrAvidin beads (Pierce) for 18–24 h at 4 °C. Bound material was eluted with sample buffer and subjected to SDS/PAGE and then immunoblotted with the indicated antibodies. Blots were then quantified using the CCD-based ChemiDoc XRS + system. Antibodies against the β3 subunit and the phospho- β3 antibody were generated and verified by the laboratory of S.J.M. (Vien et al., 2015).

3. Results

3.1. Comparing the effects of endogenous and synthetic neurosteriods on the activity of recombinant $GABA_ARs$

ALLO and ganaxolone are known PAMs of both synaptic and extrasynaptic $GABA_A$R-mediated currents. The ability of SGE-516 to act as a PAM was compared to ALLO and ganaxolone using the whole-cell recordings of recombinant human $GABA_A$ receptors expressed in mammalian cells. The α1β2γ2 or α4β3δ subunit combinations were chosen as representatives of typical synaptic and extrasynaptic $GABA_A$ receptors respectively. Similar to previous reports (Botella et al., 2015), ALLO, ganaxolone and SGE-516 allosterically potentiated currents induced by EC_{20} concentration of GABA in a concentration-dependent manner in both synaptic- and extrasynaptic-type $GABA_ARs$. ALLO potentiated α1β2γ2 receptors with an EC_{50} of 115 nM and E_{max} of 229% and potentiated α4β3δ receptors with an EC_{50} of 57 nM and E_{max} of 426%. SGE-516 potentiated α1β2γ2 receptors with an EC_{50} of 61 nM and E_{max} of 219%. Likewise, SGE-516 potentiated α4β3δ receptors with an EC_{50} of 193 nM and E_{max} of 400%. Ganaxolone potentiated α1β2γ2 receptors with an EC_{50} of 256 nM and E_{max} of 307% and potentiated α4β3δ receptors with an EC_{50} of 94 nM and E_{max} of 225% (Table 1). To confirm the presence of the γ2 subunit in α1β2γ2 receptors, we also checked the effects of diazepam, a well-known benzodiazepine PAM specifically for synaptic $GABA_ARs$ (data not shown). It was observed that diazepam potentiates the GABA evoked currents in α1β2γ2 receptors with an EC_{50} of 69 nM and E_{max} of 184%. In contrast, it did not alter GABA evoked currents in α4β3δ receptors. The results indicate that like ALLO, and ganaxolone, SGE-516 is a potent and efficacious PAM for both synaptic and extrasynaptic type $GABA_ARs$.

3.2. Acute exposure to NASs allosterically potentiates tonic current in the dentate gyrus granule cells

The results from the above experiments with synaptic-, and extrasynaptic-like $GABA_ARs$ expressed in HEK293 cells demonstrated the ability of ALLO, SGE-516, and ganaxolone to potentiate sub-maximal GABA-mediated currents. We next examined the ability of acute application of these NASs to allosterically modulate phasic and tonic currents in dentate gyrus granule cells (DGGCs) in hippocampal slices from 3 to 5 weeks old male C57/Bl6 mice. As would be expected, both ALLO, and SGE-516 modulated the tonic holding current in DGGCs in hippocampal slices (Fig. 1). At 100 nM, ALLO modulated the tonic current from 31.8 ± 5.9 pA, to 58.3 ± 13.0 pA, ($n = 5$) and 100 nM SGE-516 modulated the tonic current from 34.2 ± 11.1 pA, to 49.2 ± 8.9 ($n = 7$). The only significant modulation was observed with 100 nM ganaxolone which modulated DGGC tonic current from 42.1 ± 17.5 to 78.8 ± 23.2 pA ($n = 6$; $p = 0.004$ paired *t*-test).

3.3. Comparing the acute effects of NASs on phasic currents in DGGCs

We also compared the properties of inhibitory synaptic currents in DGGCs before and during exposure to NASs (Fig. 2). It was observed that there was no significant difference in the mean sIPSC amplitude before and during exposure with 100 nM ALLO ($p = 0.85$, $n = 5$), 100 nM SGE-516 ($p = 0.46$, $n = 7$) and 100 nM ganaxolone ($p = 0.07$, $n = 6$) (Table 2). However, the mean sIPSC decay time significantly increased in the presence of ALLO, SGE-516, and ganaxolone ($p = 0.03$, $p = 0.01$, and $p = 0.04$ respectively, Table 2).

3.4. Exposure to NASs metabotropically enhances tonic current in DGGCs

Recently we have shown that, in addition to the allosteric modulation of $GABA_A$ receptors, THDOC, exert sustained effects on

Table 1
Properties of neuroactive steroids on recombinant $GABA_ARs$.

Compound	α1β2γ2		α4β3δ	
	EC_{50} (pEC_{50} ± S.E.M.)	E_{max} ± S.E.M. (%)	EC_{50} (pEC_{50} ± S.E.M.)	E_{max} ± S.E.M. (%)
ALLO	115 (6.9 ± 0.2)	229 ± 19	57 (7.2 ± 0.3)	426 ± 42
SGE-516	61 (7.2 ± 0.3)	219 ± 21	193 (6.7 ± 0.1)	505 ± 19
Ganaxolone	256 (6.6 ± 0.2)	400 ± 27	94 (7.0 ± 0.1)	225 ± 8

EC_{50} values are given in nM with -pEC_{50} ± S.E.M., $n = 3$ for all.

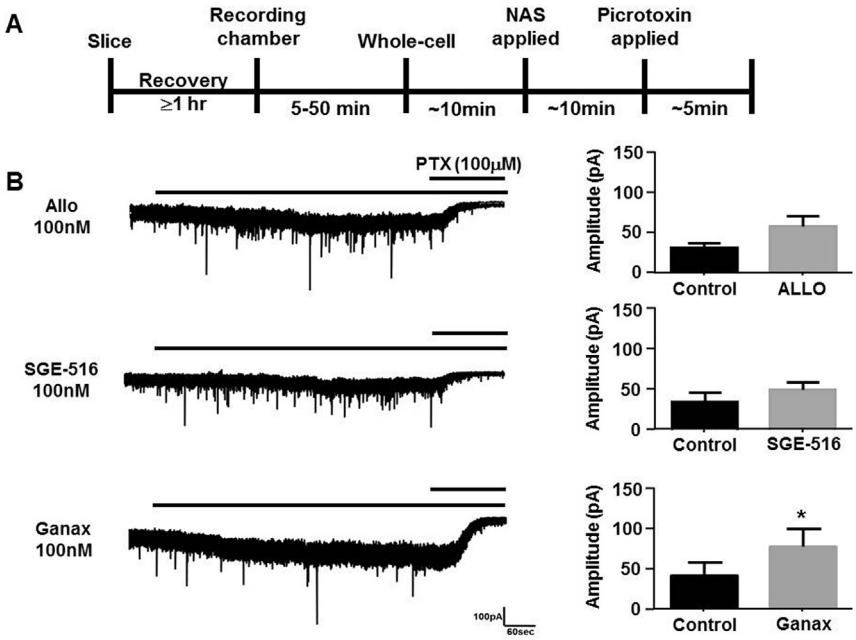

Fig. 1. NASs allosterically modulate DGGC tonic currents. A. Scheme demonstrating experimental protocol. Hippocampal slices from p21-35 (C57/Bl6) mice were allowed to recover for at least 1 h following slicing. Slices were transferred to the recording chamber of the microscope. After achieving the whole-cell configuration approximately 10 min was allowed for membrane currents to stabilize. Hippocampal slices were acutely exposed to 100 nM ALLO, SGE-516, or ganaxolone (Ganax) for 10 min followed by 100 μM picrotoxin (PTX). **B**. Example of current recordings from DGGCs showing modulation of tonic currents by acutely applied NASs (left panel). Bars above current recordings represent application of NAS and picrotoxin. Bar graphs summarizing the average tonic current (mean ± SEM) before and during acute exposure with ALLO, SGE-516, or ganaxolone (right panel). * = significantly different to control ($p = 0.004$; *t*-test), n = 4–12 cells.

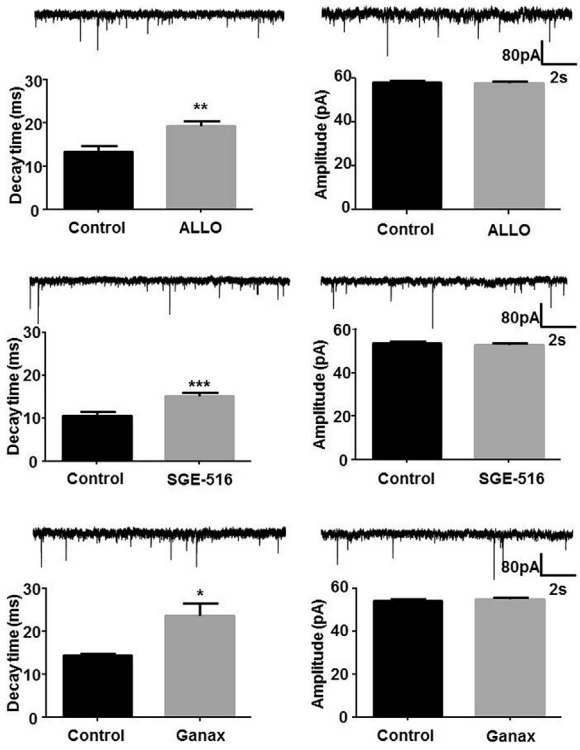

Fig. 2. Allosteric modulation of phasic currents by acutely applied NASs. Recordings of sIPSCs from DGGCs before and during acute exposure to 100 nM ALLO, 100 nM SGE-516, or 100 nM ganaxolone for 10 min. Example of current recordings from DGGCs showing phasic currents before and during acutely applied NASs (left panel). Bar graphs summarizing the effects of acute exposure of ALLO, SGE-516, or ganaxolone on the amplitude and decay of sIPSCs (right panel). ***p = 0.01, **p = 0.03, *p = 0.04, paired *t*-test, n = 5–7 cells.

GABAergic tonic current by enhancing the PKC-dependent phosphorylation of the α4 and β3 subunits, leading to enhanced insertion and stability of $GABA_A$Rs into the membrane and a long lasting increase in tonic current (Abramian et al., 2010, 2014).

Here, we analyzed the sustained effects of ALLO, or the new synthetic NAS SGE-516 on the tonic current in DGGCs in hippocampal slices from 3 to 5 week old C57 male mice. Hippocampal slices were incubated for 15 min in a chamber containing NASs dissolved in ACSF. Slices were then transferred to the recording chamber of the microscope followed by a wash period between 30 and 60 min of continuous perfusion of NAS-free ACSF before recordings were started (Fig. 3A).

Slices exposed to ALLO, or SGE-516 demonstrated a concentration-dependent increase in the tonic current measured by the addition of picrotoxin with the maximal effects at 1 μM. Control, vehicle-treated slices had a tonic current of 43.9 ± 5.7 pA (n = 12), whereas the tonic currents for slices treated with SGE-516 (1 μM) was 123.0 ± 22.2 pA, (n = 6, p = 0.0003), or ALLO (1 μM) was 95.8 ± 10.8 pA (n = 4, p = 0.0005, Fig. 3B&C).

In addition, we also examined if the synthetic NAS, ganaxolone, also had a metabotropic effect following 15 min incubation. In contrast to the naturally occurring NASs THDOC, and ALLO, and the synthetic NAS, SGE-516, ganaxolone (1 μM) did not significantly alter the magnitude of tonic current in DGGCs (57.4 ± 6.3 pA, n = 7, p = 0.14, Fig. 3D).

To assess if the effects of NASs are dependent upon PKC, hippocampal slices were treated with the established PKC inhibitor GF 109203X (GFX 50 μM) for 15 min followed by co-exposure of to ALLO, or SGE-516 and GFX for 15 min. When tonic current was measured following ≥30 min washout, there was no significant difference to the tonic current measured in ALLO/GFX, or SGE-516/GFX treated slices with vehicle treated slices (Fig. 3).

We measured the tonic current by blocking extrasynaptic $GABA_A$Rs with picrotoxin. Because picrotoxin also inhibits glycine

Table 2
Allosteric modulation of DGGC sIPSCs evoked by 100 nM ALLO, SGE-516, and ganaxolone.

sIPSC	Control	ALLO	Control	SGE-516	Control	Ganax
Amplitude (pA)	59.2 ± 0.7	59.1 ± 0.6	53.7 ± 0.7	52.9 ± 0.7	54.2 ± 0.6	55.1 ± 0.7
Frequency (Hz)	4.5 ± 0.9	3.4 ± 1.0	4.1 ± 0.4	4.6 ± 0.6	6.4 ± 1.3	5.6 ± 1.7
Decay (ms)	13.4 ± 1.3	19.2 ± 1.3[b]	10.5 ± 1.1	15.1 ± 0.8[a]	14.4 ± 0.5	23.6 ± 2.9[c]

Data is mean SEM, n = 5 to 7 neurons.
[a] p = 0.01.
[b] p = 0.03.
[c] p = 0.04.

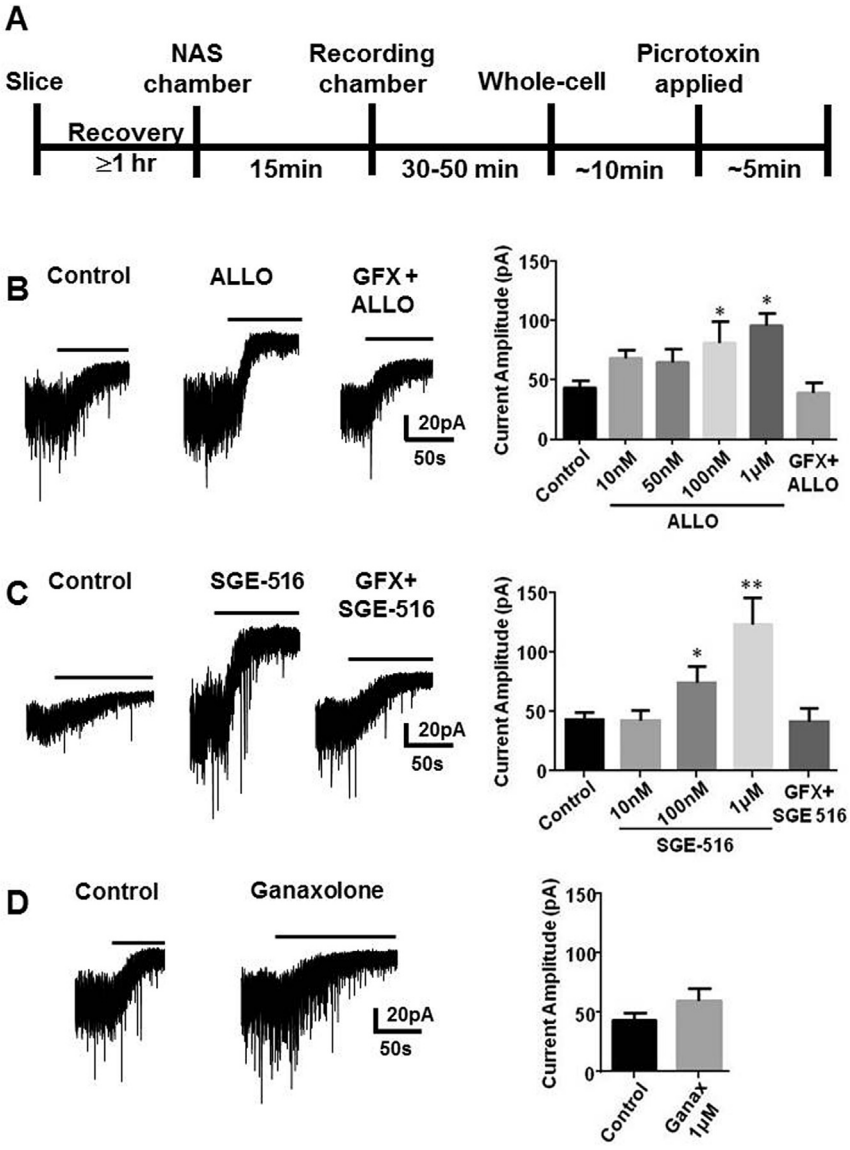

Fig. 3. NAS-mediated metabotropic enhancement of tonic inhibitory current in DGGC neurons. A. Scheme demonstrating experimental protocol. Hippocampal slices were allowed to recover for at least 1 h following slicing. Slices were then incubated for 15 min in a chamber containing NASs dissolved in ACSF. Slices were then transferred to the recording chamber of the microscope followed by a wash period between 30 and 60 min of continuous perfusion of NAS-free ACSF before recordings were started. Recordings were made from DGGCS in hippocampal slices from p21-35 C57 mice in the presence of 5 μM GABA followed by 100 μM picrotoxin and the difference in holding current was then determined. **Left panel B, C, D**. Example tonic currents from slices following exposures to vehicle (control) or 100 nM ALLO (B), 100 nM SGE-516 (C), or 1 μM ganaxolone (D) for 15 min. No change in tonic current was observed in slices pre-incubated for 15 min with GFX followed by ALLO, or SGE-516. Bar above current represents application of picrotoxin (100 μM). **Right panel B, C, D**. Bar graph shows average tonic current was significantly enhanced following exposure to different concentrations of ALLO and SGE-516. No significant change in tonic current was observed following exposure to 1 μM ganaxolone for 15 min. In all panels * = significantly different to control ($p < 0.05$; un-paired *t*-test, n = 4–12 cells).

receptors we examined if glycine receptors contributed to tonic current by using the specific glycine receptor inhibitor, strychnine. There was no difference in tonic current measured under control conditions in the absence or presence of strychnine (100 nM). Similarly, there was no difference in the increase in tonic current following a 15 min exposure to 100 nM ALLO in the absence or

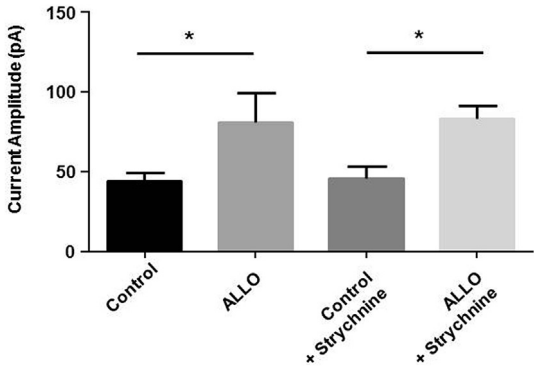

Fig. 4. Glycine receptors do not contribute to tonic current in DGGCs. Hippocampal slices were incubated for 15 min with 100 nM ALLO or vehicle dissolved in ACSF then transferred to the recording chamber and washed for 30–60 min with NAS-free ACSF before recordings were started. Tonic current was measured by applying 100 μM picrotoxin in the absence or presence of the glycine receptor, strychnine (100 nM). Exposure to ALLO caused a significant increase in tonic current. Addition of strychnine did not alter the tonic current measured with picrotoxin. *p = 0.01, unpaired *t*-test, n = 4–12 neurons.

presence of strychnine (Fig. 4). These results suggest that glycine receptors have an undetected contribution to tonic current in DGGCs and that the metabotropic increase in tonic current by NAS exposure do not involve glycine receptors.

Collectively, these results suggest that the exposure of hippocampal slices to SGE-516 and ALLO has a strong sustained metabotropic effects on tonic current. In contrast, ganaxolone produce major effects via allosteric mechanism as compared to metabotropic effects.

3.5. The metabotropic effects of NASs on phasic current in DGGCs

In parallel with our measurements on tonic current we assessed the effects of prior exposure of NASs on sIPSC properties. The amplitude of sIPSCs was significantly increased after incubation with 100 nM SGE-516 compared to vehicle control (control 39 ± 0.9 pA, n = 12; SGE-516 58 ± 1.9 pA, n = 6, p = 0.0001). This increase in sIPSC amplitude following exposure to SGE-516 was significantly reduced following co-exposure with SGE-516 and GFX (Fig. 5C). No change in sIPSC amplitude was observed following exposure with 100 nM ALLO or 1 μM ganaxolone (Fig. 5B&D). In

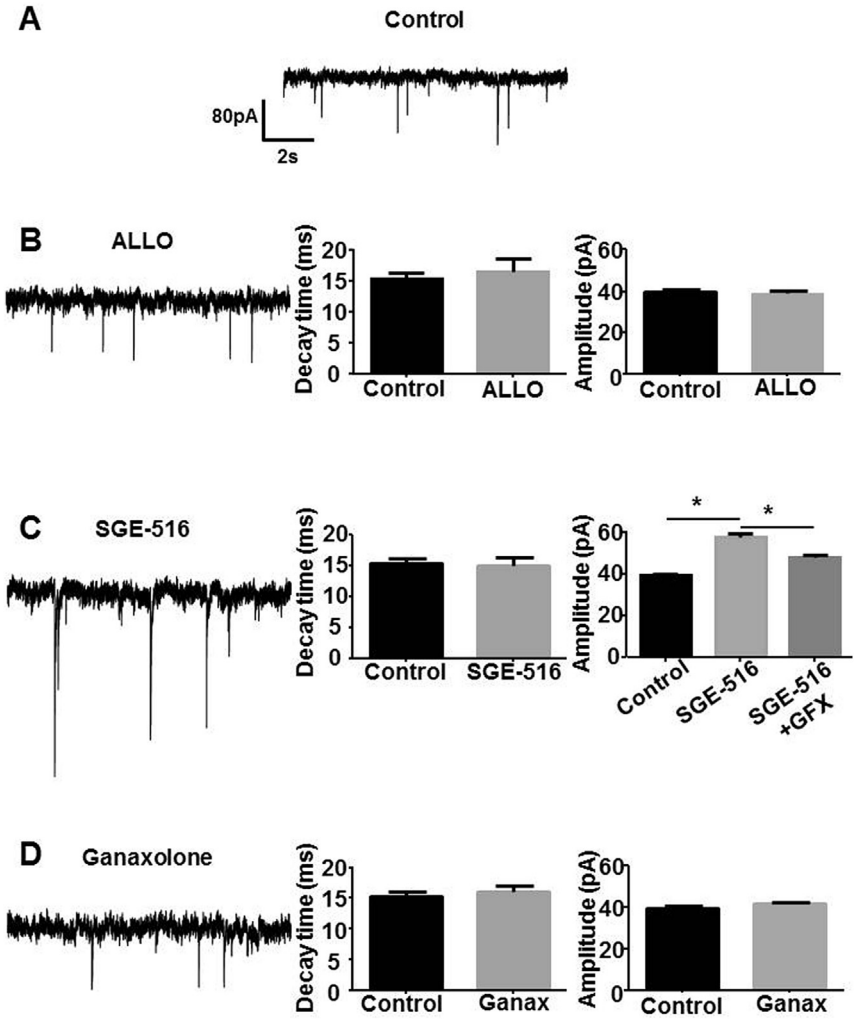

Fig. 5. sIPSC amplitude and decay was largely uncharged following exposure to NASs. A. IPSC recordings were made from DGGCS in hippocampal slices from p21-35 C57 mice. The slices were exposed to vehicle (control, n = 6 neurons from 3 mice), **B**.100 nM ALLO (n = 4 neurons from, 2 mice), **C**.100 nM SGE-516 (n = 5 neurons from 2 mice), or **D**. 1 μM ganaxolone (n = 5 neurons from 2 mice) for 15 min and then washed for >30 min prior to measurement of sIPSCs. Bar graphs shows average sIPSC decay and amplitude. Only sIPSC amplitude was significantly enhanced following exposure to 100 nM SGE-516 but GFX (n = 5 neurons from 2 mice) significantly reduced SGE-516 enhancement. * = significantly different to control (p < 0.05; unpaired *t*-test).

contrast to the changes observed with the allosteric modulation of IPSC decay time, no metabotropic-mediated changes in sIPSC decay time was observed following exposure to ALLO, SGE-516, or ganaxolone (Fig. 5).

3.6. SGE-516 and ALLO increase the phosphorylation and cell surface stability of $GABA_ARs$

We have previously shown that the naturally occurring NAS, THDOC, increased tonic current in part through phosphorylation of S408/409 of the β3 subunit (Abramian et al., 2014; Vien et al., 2015). To further our understanding of the NAS-mediated increase in tonic current we measured the effects of ALLO, SGE-516, on the phosphorylation and membrane expression of β3 subunits in hippocampal slices. Twenty min exposure to 100 nM ALLO, or SGE-516 increased phosphorylation of β3 subunits at S408/409 to 141 ± 10% of control ($n = 10$, $p < 0.01$), and 143± 14% of control ($n = 4$, $p < 0.05$) respectively (Fig. 6A&B).

In parallel with modulating phosphorylation, exposure to 100 nM ALLO, or SGE-516 increased the cell surface expression levels of receptors containing β3 subunits to 166± 22% of control ($n = 8$, $p < 0.05$), and 180 ± 29% of control ($n = 4$, $p < 0.05$) respectively (Fig. 6C&D). Therefore, in parallel with inducing sustained effects on GABAergic inhibition ALLO and SGE-516 enhance the cell surface levels and phosphorylation of the $GABA_ARs$ containing β3 subunits dependent upon PKC activity.

4. Discussion

We have previously shown that the endogenous NAS, THDOC, exerts a sustained increase on GABAergic tonic current in cultured neurons. The THDOC-mediated increase in α4/β3 subunit-mediated current is independent of the allosteric potentiation typically described of NASs. Rather, we described a metabotropic signaling mechanism by which THDOC induced a PKC-mediated phosphorylation of α4 and β3 subunits with a subsequent increase in the insertion of $GABA_ARs$, and a reduction in their endocytosis (Abramian et al., 2010, 2014; Adams et al., 2015). Here we have assessed this putative regulatory mechanism for other endogenous and synthetic NASs in the dentate gyrus.

To do so, hippocampal slices were exposed to NAS for 15 min followed by ≥ 30 min wash in a separate recording chamber before the start of the experiment. Both ALLO and SGE-516 significantly enhanced the tonic current compared to vehicle treated slices via a metabotropic mechanism. This is in contrast with the non-significant allosteric enhancement of tonic current we observed with ALLO and SGE-516. However, we also examined the first generation synthetic NAS, ganaxolone, and although it significantly produced an allosteric potentiated tonic current it failed to metabotropically modulate tonic current. This result demonstrates that the metabotropic pathway that increases the PKC-mediated phosphorylation of α4 and β3 subunits can be stimulated by both endogenous and synthetic NASs but is not universally stimulated by all steroids.

Ganaxolone, ALLO, and SGE-516 all allosterically prolonged the decay of sIPSCs, and allosterically potentiated recombinant $GABA_ARs$ demonstrating their recognized role as $GABA_ARs$ PAMs. However, in our metabotropic studies only SGE-516 significantly altered sIPSC properties, with an increase in sIPSC amplitude. Our previous data has demonstrated the link between PKC-mediated phosphorylation of β3 subunits with a subsequent reduction in $GABA_AR$ endocytosis and an increase in IPSC amplitude (Jovanovic et al., 2004; Kittler et al., 2005; Vien et al., 2015).

In DGGCs, from mice that are 3 weeks and older the predominant extrasynaptic combination is thought to be α4βnδ or even just α4βn (Bencsits et al., 1999; Chandra et al., 2006; Mortensen and Smart, 2006). Extrasynaptic $GABA_ARs$ in hippocampal CA1 pyramidal neurons have the α5 subunit whereas, extrasynaptic $GABA_ARs$ in hippocampal interneurons are comprised of α1βnδ subunits (Caraiscos et al., 2004; Glykys et al., 2007). We have

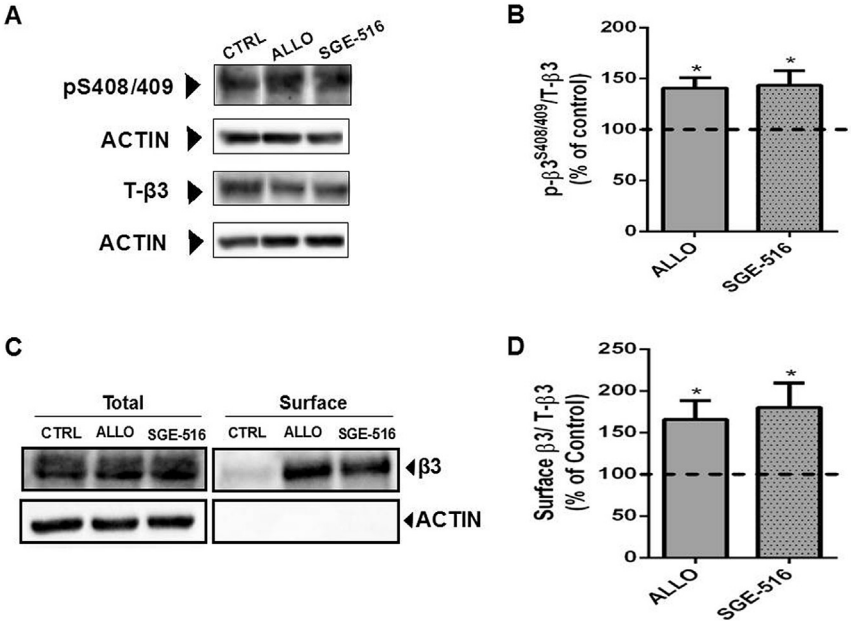

Fig. 6. NAS exposure increases phosphorylation and surface expression of β3 subunits. A. Exposure to 100 nM of the NASs, ALLO or SGE-516, for 20 min increases β3 S408/409 phosphorylation in acute hippocampal slices. **B**. The ratio of p-β3/T-β3 was measured and values were normalized to those in control (100%). Asterisks represent a significant difference from control (ALLO: $p < 0.01$, Student's *t*-test, $n = 10$ slices, from 10 mice; SGE-516: $p < 0.05$, Student's *t*-test, $n = 4$ slices, from 4 mice). **C**. Exposure to 100 nM ALLO or SGE-516 for 20 min increases $GABA_A$-β3–containing receptors at the plasma membrane in acute hippocampal slices. **D**. The ratio of surface β3/T-β3 was measured and values were normalized to cell surface levels in control treated slices (100%). Asterisks represent a significant difference from control (ALLO: $p < 0.05$, Student's *t*-test, $n = 8$ slices; SGE-516: $p < 0.05$, Student's *t*-test, $n = 4$ slices).

previously shown that with NAS exposure, α5 and α1 subunits are not phosphorylated nor is there an increase in α5 and α1 subunit trafficking to the membrane surface (Abramian et al., 2014). We have only observed the NAS-evoked PKC-dependent increase in tonic current through the phosphorylation of α4 and β3 subunits and this phosphorylation occurs independently of the presence of δ subunits (Abramian et al., 2014), suggesting a brain region selective change in extrasynaptic $GABA_AR$ trafficking. Extrasynaptic $GABA_ARs$ in dentate gyrus granule cells have been suggested to be a mix of α4β2δ and α4β3δ subunits (Herd et al., 2008). $GABA_ARs$ comprised of α4β2δ have been shown to undergo increased endocytosis upon PKC phosphorylation of β2 S410 (Bright and Smart, 2013). A hypothetical consequence of NAS-mediated increase in PKC phosphorylation of $GABA_A$ subunits would be the predominance of extrasynaptic $GABA_ARs$ comprised of α4β3δ subunits.

Reduced expression of extrasynaptic $GABA_ARs$ has been demonstrated in human and rodent models of postpartum depression, schizophrenia, epilepsies, Angelman, Rett, and Fragile X syndromes (Curia et al., 2009; D'Hulst and Kooy, 2007; Gantois et al., 2006; Maguire and Mody, 2008; Maldonado-Aviles et al., 2009). We have previously described a decrease in phosphorylation of residues S408/409 of the β3 subunit following status epilepticus leading to an increase in $GABA_AR$ endocytosis and increased excitation (Terunuma et al., 2008). Thus, by increasing the phosphorylation of the β3 subunit by exposure to NAS the expression and trafficking of these extrasynaptic $GABA_AR$ subunits could be manipulated and may provide novel therapeutic areas for these difficult to treat disorders.

The NAS-mediated increase in phosphorylation and surface levels of extrasynaptic $GABA_ARs$ leading to an increase in tonic current is a further mechanism by which NASs can increase the inhibitory tone in the brain in addition to the more commonly described allosteric effect. While the allosteric modulation only exists while the NAS is present, the PKC-mediated metabotropic enhancement can cause a prolonged increase in inhibitory tone. We have noted before that other positive allosteric modulators such as the intravenous general anesthetic, propofol, do not have the ability to metabotropically enhance extrasynaptic $GABA_ARs$ (Abramian et al., 2014). Here, we have demonstrated that not all steroidal modulators (ganaxolone) have the ability to increase tonic current through this metabotropic mechanism either. However, the metabotropic pathway seems to be activated by various NAS including endogenous THDOC, and ALLO and the synthetic NAS, SGE-516. The activation of this pathway increases phosphorylation of the β3 subunit, leading to increased surface expression of the receptor and an increase in tonic current. All of which leads to an interesting area of potential therapeutic targets aimed at modulating the trafficking of a particularly important subset of $GABA_ARs$.

Conflicts of interest

The authors declare that they have no conflicts of interest with the contents of this article. The content is solely the responsibility of the authors and does not necessarily represent the official views of the National Institutes of Health. SJM serves as a consultant for SAGE therapeutics and AstraZeneca, relationships that are regulated by Tufts University and do not impact on this study. JJD and MAA are employees of SAGE therapeutics.

Author contributions

AM performed and analyzed the patch clamp experiments and drafted the paper, MLP performed phosphorylation and biotinylation experiments and drafted the paper, MAA conceived and coordinated the study, JJD conceived and coordinated the study, SJM conceived and coordinated the study, and wrote the paper PAD conceived and coordinated the study and wrote the paper.

Acknowledgements

This work was supported by grants from the National Institutes of Health (NIH)-National Institute of Alcoholism and Alcohol Abuse grant AA017938 (P.A.D), NIH-National Institute of Mental Health grant, MH097446, and DOD, AR140209 (PAD & SJM), NIH-National Institute of Neurological Disorders and Stroke grant NS051195, NS056359, NS081735, NS080064, NS087662 (SJM), the Simons Foundation #206026 (S.J.M.).

References

Abramian, A.M., Comenencia-Ortiz, E., Modgil, A., Vien, T.N., Nakamura, Y., Moore, Y.E., Maguire, J.L., Terunuma, M., Davies, P.A., Moss, S.J., 2014. Neurosteroids promote phosphorylation and membrane insertion of extrasynaptic GABAA receptors. Proc. Natl. Acad. Sci. U. S. A. 111, 7132–7137.

Abramian, A.M., Comenencia-Ortiz, E., Vithlani, M., Tretter, E.V., Sieghart, W., Davies, P.A., Moss, S.J., 2010. Protein kinase C phosphorylation regulates membrane insertion of GABAA receptor subtypes that mediate tonic inhibition. J. Biol. Chem. 285, 41795–41805.

Adams, J.M., Thomas, P., Smart, T.G., 2015. Modulation of neurosteroid potentiation by protein kinases at synaptic- and extrasynaptic-type GABAA receptors. Neuropharmacology 88, 63–73.

Belelli, D., Harrison, N.L., Maguire, J., Macdonald, R.L., Walker, M.C., Cope, D.W., 2009. Extrasynaptic GABAA receptors: form, pharmacology, and function. J. Neurosci. 29, 12757–12763.

Bencsits, E., Ebert, V., Tretter, V., Sieghart, W., 1999. A significant part of native gamma-aminobutyric AcidA receptors containing alpha4 subunits do not contain gamma or delta subunits. J. Biol. Chem. 274, 19613–19616.

Botella, G.M., Salituro, F.G., Harrison, B.L., Beresis, R.T., Bai, Z., Shen, K.S., Belfort, G.M., Loya, C.M., Ackley, M.A., Grossman, S.J., Hoffmann, E., Jia, S.L., Wang, J.M., Doherty, J.J., Robichaud, A.J., 2015. Neuroactive steroids. 1. Positive allosteric modulators of the (gamma-aminobutyric acid)(A) receptor: structure-activity relationships of heterocyclic substitution at C-21. J. Med. Chem. 58, 3500–3511.

Brickley, S.G., Mody, I., 2012. Extrasynaptic GABA(A) receptors: their function in the CNS and implications for disease. Neuron 73, 23–34.

Bright, D.P., Smart, T.G., 2013. Protein kinase C regulates tonic GABA(A) receptor-mediated inhibition in the hippocampus and thalamus. Eur. J. Neurosci. 38, 3408–3423.

Caraiscos, V.B., Elliott, E.M., You-Ten, K.E., Cheng, V.Y., Belelli, D., Newell, J.G., Jackson, M.F., Lambert, J.J., Rosahl, T.W., Wafford, K.A., MacDonald, J.F., Orser, B.A., 2004. Tonic inhibition in mouse hippocampal CA1 pyramidal neurons is mediated by alpha5 subunit-containing gamma-aminobutyric acid type A receptors. Proc. Natl. Acad. Sci. U. S. A. 101, 3662–3667.

Chandra, D., Jia, F., Liang, J., Peng, Z., Suryanarayanan, A., Werner, D.F., Spigelman, I., Houser, C.R., Olsen, R.W., Harrison, N.L., Homanics, G.E., 2006. GABAA receptor alpha 4 subunits mediate extrasynaptic inhibition in thalamus and dentate gyrus and the action of gaboxadol. Proc. Natl. Acad. Sci. U. S. A. 103, 15230–15235.

Curia, G., Papouin, T., Seguela, P., Avoli, M., 2009. Downregulation of tonic GABAergic inhibition in a mouse model of fragile X syndrome. Cereb. Cortex 19, 1515–1520.

D'Hulst, C., Kooy, R.F., 2007. The GABAA receptor: a novel target for treatment of fragile X? Trends Neurosci. 30, 425–431.

Gantois, I., Vandesompele, J., Speleman, F., Reyniers, E., D'Hooge, R., Severijnen, L.A., Willemsen, R., Tassone, F., Kooy, R.F., 2006. Expression profiling suggests underexpression of the GABA(A) receptor subunit delta in the fragile X knockout mouse model. Neurobiol. Dis. 21, 346–357.

Glykys, J., Mody, I., 2007. Activation of GABAA receptors: views from outside the synaptic cleft. Neuron 56, 763–770.

Glykys, J., Peng, Z., Chandra, D., Homanics, G.E., Houser, C.R., Mody, I., 2007. A new naturally occurring GABA(A) receptor subunit partnership with high sensitivity to ethanol. Nat. Neurosci. 10, 40–48.

Herd, M.B., Haythornthwaite, A.R., Rosahl, T.W., Wafford, K.A., Homanics, G.E., Lambert, J.J., Belelli, D., 2008. The expression of GABAA beta subunit isoforms in synaptic and extrasynaptic receptor populations of mouse dentate gyrus granule cells. J. Physiol. 586, 989–1004.

Jovanovic, J.N., Thomas, P., Kittler, J.T., Smart, T.G., Moss, S.J., 2004. Brain-derived neurotrophic factor modulates fast synaptic inhibition by regulating GABA(A) receptor phosphorylation, activity, and cell-surface stability. J. Neurosci. 24, 522–530.

Kittler, J.T., Chen, G., Honing, S., Bogdanov, Y., McAinsh, K., Arancibia-Carcamo, I.L., Jovanovic, J.N., Pangalos, M.N., Haucke, V., Yan, Z., Moss, S.J., 2005. Phospho-dependent binding of the clathrin AP2 adaptor complex to GABAA receptors regulates the efficacy of inhibitory synaptic transmission. Proc. Natl. Acad. Sci. U. S. A. 102, 14871–14876.

Kretschmannova, K., Hines, R.M., Revilla-Sanchez, R., Terunuma, M., Tretter, V., Jurd, R., Kelz, M.B., Moss, S.J., Davies, P.A., 2013. Enhanced tonic inhibition influences the hypnotic and amnestic actions of the intravenous anesthetics etomidate and propofol. J. Neurosci. 33, 7264–7273.
Maguire, J., Mody, I., 2008. GABA(A)R plasticity during pregnancy: relevance to postpartum depression. Neuron 59, 207–213.
Maldonado-Aviles, J.G., Curley, A.A., Hashimoto, T., Morrow, A.L., Ramsey, A.J., O'Donnell, P., Volk, D.W., Lewis, D.A., 2009. Altered markers of tonic inhibition in the dorsolateral prefrontal cortex of subjects with schizophrenia. Am. J. Psychiatry 166, 450–459.
Mitchell, E.A., Herd, M.B., Gunn, B.G., Lambert, J.J., Belelli, D., 2008. Neurosteroid modulation of GABAA receptors: molecular determinants and significance in health and disease. Neurochem. Int. 52, 588–595.
Mortensen, M., Smart, T.G., 2006. Extrasynaptic alphabeta subunit GABAA receptors on rat hippocampal pyramidal neurons. J. Physiol. 577, 841–856.
Nusser, Z., Mody, I., 2002. Selective modulation of tonic and phasic inhibitions in dentate gyrus granule cells. J. Neurophysiol. 87, 2624–2628.
Paul, S.M., Purdy, R.H., 1992. Neuroactive steroids. FASEB J. 6, 2311–2322.
Rupprecht, R., 2014. New perspectives in neurosteroid action: open questions for future research. Front. Cell Neurosci. 8, 268.
Semyanov, A., Walker, M.C., Kullmann, D.M., Silver, R.A., 2004. Tonically active GABA A receptors: modulating gain and maintaining the tone. Trends Neurosci. 27, 262–269.
Terunuma, M., Xu, J., Vithlani, M., Sieghart, W., Kittler, J., Pangalos, M., Haydon, P.G., Coulter, D.A., Moss, S.J., 2008. Deficits in phosphorylation of GABA(A) receptors by intimately associated protein kinase C activity underlie compromised synaptic inhibition during status epilepticus. J. Neurosci. 28, 376–384.
Vien, T.N., Modgil, A., Abramian, A.M., Jurd, R., Walker, J., Brandon, N.J., Terunuma, M., Rudolph, U., Maguire, J., Davies, P.A., Moss, S.J., 2015. Compromising the phosphodependent regulation of the GABAAR beta3 subunit reproduces the core phenotypes of autism spectrum disorders. Proc. Natl. Acad. Sci. U. S. A. 112, 14805–14810.

Compromising the phosphodependent regulation of the $GABA_AR$ β3 subunit reproduces the core phenotypes of autism spectrum disorders

Thuy N. Vien[a], Amit Modgil[a], Armen M. Abramian[a], Rachel Jurd[a], Joshua Walker[a], Nicholas J. Brandon[b], Miho Terunuma[c], Uwe Rudolph[d], Jamie Maguire[a], Paul A. Davies[a], and Stephen J. Moss[a,e,1]

[a]Department of Neuroscience, Tufts University School of Medicine, Boston, MA 02111; [b]AstraZeneca Neuroscience iMed, Cambridge, MA 02139; [c]Department of Cell Physiology and Pharmacology, University of Leicester, Leicester LE1 9HN, United Kingdom; [d]Laboratory of Genetic Neuropharmacology, McLean Hospital, and Department of Psychiatry, Harvard Medical School, Belmont, MA 02478; and [e]Department of Neuroscience, Physiology, and Pharmacology, University College, London WC1E 6BT, United Kingdom

Edited by Richard L. Huganir, The Johns Hopkins University School of Medicine, Baltimore, MD, and approved October 22, 2015 (received for review July 24, 2015)

Alterations in the efficacy of neuronal inhibition mediated by $GABA_A$ receptors ($GABA_ARs$) containing β3 subunits are continually implicated in autism spectrum disorders (ASDs). In vitro, the plasma membrane stability of $GABA_ARs$ is potentiated via phosphorylation of serine residues 408 and 409 (S408/9) in the β3 subunit, an effect that is mimicked by their mutation to alanines. To assess if modifications in β3 subunit expression contribute to ASDs, we have created a mouse in which S408/9 have been mutated to alanines (S408/9A). S408/9A homozygotes exhibited increased phasic, but decreased tonic, inhibition, events that correlated with alterations in the membrane stability and synaptic accumulation of the receptor subtypes that mediate these distinct forms of inhibition. S408/9A mice exhibited alterations in dendritic spine structure, increased repetitive behavior, and decreased social interaction, hallmarks of ASDs. ASDs are frequently comorbid with epilepsy, and consistent with this comorbidity, S408/9A mice exhibited a marked increase in sensitivity to seizures induced by the convulsant kainic acid. To assess the relevance of our studies using S408/9A mice for the pathophysiology of ASDs, we measured S408/9 phosphorylation in *Fmr1* KO mice, a model of fragile X syndrome, the most common monogenetic cause of ASDs. Phosphorylation of S408/9 was selectively and significantly enhanced in *Fmr1* KO mice. Collectively, our results suggest that alterations in phosphorylation and/or activity of β3-containing $GABA_ARs$ may directly contribute to the pathophysiology of ASDs.

GABA receptor | phosphorylation | autism spectrum disorder | tonic inhibition | phasic inhibition

$GABA_A$ receptors ($GABA_ARs$) are Cl^- selective ligand-gated ion channels that mediate phasic and tonic inhibition in the adult brain. Consistent with their roles in limiting neuronal excitability, benzodiazepines, barbiturates, general anesthetics, and neurosteroids exert their anxiolytic, anticonvulsant, hypnotic, and sedative effects via potentiating $GABA_AR$ activity (1). $GABA_ARs$ are heteropentamers constructed from α1–6, β1–3, γ1–3, δ, ε, θ, and π subunits. Phasic inhibition is principally mediated by receptors assembled from α1–3, β1–3, and γ2 subunits, whereas those receptors that mediate tonic inhibition contain α4–6, β1–3, and δ subunits (2). Studies using KO mice have shown that the β3 subunit is an essential component of receptor subtypes that mediate phasic and tonic inhibition (3). Together with the *Fmr1* gene (Fragile X mental retardation), mutations to the 15q11–13 locus, where the $GABA_AR$ β3 gene resides, are the leading monogenetic causes of autism spectrum disorders (ASDs) (4). Moreover, β3 subunit mutations have been described in seizure disorders, and alterations in subunit expression levels have also been reported in ASDs (3, 5).

In vitro studies have revealed that the β3 subunit plays a critical role in regulating the plasma membrane accumulation and synaptic targeting of $GABA_ARs$ via phosphorylation of the intracellular serine residues 408 and 409 (S408/9) (6, 7). S408/9 are substrates of cAMP-dependent PKA, PKC, Ca^{2+}-calmodulin type 2-dependent protein kinases (Cam KIIs), and cGMP-dependent protein kinase, and they are principally dephosphorylated by protein phosphatase 2A (8). S408/9 are the principal mediators of high-affinity binding to the clathrin adaptor molecule AP2 within the β3 subunit, and thereby facilitate $GABA_AR$ endocytosis (9). Phosphorylation of S408/9 reduces the affinity of the β3 subunit for AP2 by 100-fold, and mutation of S408/9 to alanine residues (S408/9A) has been shown to mimic the effects of phosphorylation on AP2 binding to the β3 subunit (9, 10). Accordingly, overexpression of the mutant β3 S408/9A subunit in cultured hippocampal neurons leads to an increase in the number and size of inhibitory synapses (7).

Studies in animal models of ASDs have reported modifications in the expression levels of some $GABA_AR$ mRNAs and proteins (11, 12). However, the mechanisms underlying these alterations in subunit expression and if they contribute to ASDs remain to be addressed. Therefore, in this study, we have analyzed the role that modified β3 subunit phosphorylation may play in the pathophysiology of ASDs. To test this role, we created a

Significance

Alterations in the efficacy of neuronal inhibition mediated by $GABA_A$ receptors ($GABA_ARs$) containing β3 subunits are continually implicated in autism spectrum disorders (ASDs). In vitro, the plasma membrane stability of $GABA_ARs$ is potentiated via phosphorylation of serine residues 408 and 409 (S408/9) in the β3 subunit, an effect that is mimicked by their mutation to alanines. Here, we created a mouse in which S408/9 have been mutated to alanines (S408/9A). S408/9A mice exhibited altered dendritic spine structure, increased repetitive behavior, decreased social interaction, and an epileptic phenotype. Thus, mutation of S408/9 reproduces the core deficits seen in humans with ASDs. Collectively, our results suggest that alterations in phosphorylation and/or activity of β3-containing $GABA_ARs$ may directly contribute to the pathophysiology of ASDs.

Author contributions: T.N.V., A.M., A.M.A., R.J., J.W., M.T., U.R., and J.M. designed research; T.N.V., A.M., A.M.A., R.J., J.W., N.J.B., M.T., U.R., and J.M. performed research; A.M.A., M.T., and U.R. contributed new reagents/analytic tools; T.N.V., A.M., A.M.A., R.J., J.W., N.J.B., M.T., U.R., J.M., and P.A.D. analyzed data; and T.N.V., N.J.B., U.R., J.M., P.A.D., and S.J.M. wrote the paper.

Conflict of interest statement: S.J.M. serves as a consultant for AstraZeneca and SAGE Therapeutics, relationships that are regulated by Tufts University and do not have an impact on this study.

This article is a PNAS Direct Submission.

[1]To whom correspondence should be addressed. Email: stephen.moss@tufts.edu.

This article contains supporting information online at www.pnas.org/lookup/suppl/doi:10.1073/pnas.1514657112/-/DCSupplemental.

mouse in which the principal sites of phosphodependent regulation within the receptor β3 subunit, S408/9, have been mutated to S408/9A, a mutation that mimics the effects of their phosphorylation. S408/9A mice exhibited increased phasic but decreased tonic inhibition events, which correlated with alterations in the membrane stability of the receptor subtypes that mediate these distinct forms of inhibition. S408/9A mice exhibited alterations in dendritic spine structure, increased repetitive-like behavior, and decreased social interaction, which are hallmarks of ASDs. Therefore, our results provide evidence that alterations in the activity of $GABA_A$Rs containing β3 subunits directly contribute to ASDs.

Results

Creation of a S408/9A Knock-In Mouse. Alterations in the efficacy of GABAergic inhibition mediated by β3-containing $GABA_A$Rs are strongly linked to ASDs. Phosphorylation of $GABA_A$Rs regulates their exocytosis and endocytosis, and thereby their residence time on the neuronal plasma membrane and accumulation at inhibitory synapses (8). Central to these regulatory processes is the phosphorylation of S408/9 in the β3 subunit, which reduces the affinity of $GABA_A$Rs for the clathrin adaptor protein AP2, as measured by using synthetic peptides corresponding to the β3 subunit and purified AP2 (9, 13). The significance of these findings has recently been questioned by studies that suggest that the arginine residues flanking S408/9 are the principal determinants of AP2 binding in the β3 subunit (14). To examine the significance of S408/9 further, we expressed the intracellular domain of the β3 subunit as a GST fusion protein (GSTβ3) or a fusion protein in which the respective residues were mutated to alanines (GSTβ3S408/9A) in *Escherichia coli.* The respective fusion proteins were then phosphorylated in vitro using purified PKC to final stoichiometries of ∼0.35 and ∼0.03 mol/mol, respectively, and then exposed to the μ2 subunit of AP2 (15) (Fig. S1*A*). Phosphorylation of GSTβ3 significantly reduced μ2 binding, whereas phosphorylation of GSTβ3S408/9A was without effect. Likewise GSTβ3S408/9A bound significantly lower levels of μ2 compared with GSTβ3. Collectively, these results suggest a key role for S408/9 and their phosphorylation in determining the affinity of $GABA_A$Rs for AP2 (Fig. S1 *A* and *B*).

To assess the significance of β3 subunit phosphorylation in determining the efficacy of GABAergic inhibition, we created a knock-in mouse in which S408/9 were mutated to S408/9A using homologous recombination in ES cells (Fig. S1 *C* and *D*). Mutation of the respective codons in exon 9 of the β3 subunit was confirmed by DNA sequencing (Fig. S1 *C* and *D*), and the respective mice were backcrossed on the C57BL/6J background in excess of 10 generations. S408/9A homozygotes were viable and bred normally and did not exhibit any overt phenotypes. Likewise, there did not appear to be any gross anatomical changes in the structure of the hippocampus (Fig. S1*E*). In hippocampal slices from WT mice, treatment with the PKC activator phorbol 12,13-dibutyrate produced a large increase in pS408/9 immunoreactivity, an effect not replicated in S408/9A mice (Fig. 1*A*). To control for possible global changes in $GABA_A$R phosphorylation mice, we analyzed phosphorylation of Y367 in the γ2 subunit, an accepted substrate of Src family kinases (16). Treatment of slices with vanadate, an inhibitor of tyrosine phosphatases, induced similar increases in Y367 phosphorylation in WT and S408/9A mice (Fig. 1*A*).

Characterization of $GABA_A$R expression levels and synaptic targeting in S408/9A mice. Next, we examined the effects of the S408/9A mutation on the cell surface accumulation of the $GABA_A$Rs using biotinylation. The S408/9A mutation increased the cell surface expression levels of the β3 subunit to 145 ± 8% of WT ($P < 0.05$, $n = 4$ mice of each genotype; Fig. 1*B*) without modifying total subunit expression levels ($P > 0.05$, $n = 4$ mice of each genotype; Fig. 1*C*). In the dentate gyrus, phasic inhibition is mediated by $GABA_A$R assembled from of α1/2, β2, β3, and γ2 subunits, whereas subtypes containing α4–6, β2, β3, and δ subunits are responsible for tonic current. Therefore, we assessed the effects of the S408/9 mutation on the plasma membrane accumulation of the receptor α2 and α4 subunits. The plasma membrane levels of the α2 subunit were increased in S408/9A mice to 119.0 ± 5.2% of control ($P < 0.05$, $n = 5$–6 mice of each genotype; Fig. 1*B*). In

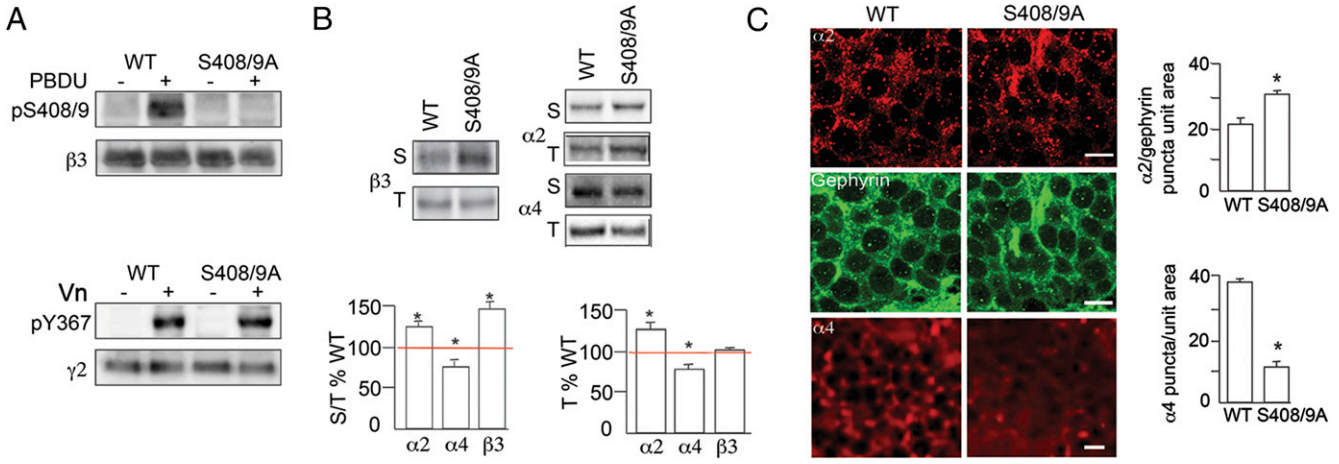

Fig. 1. $GABA_A$R expression in S408/9A mice. (*A*) Treatment of hippocampal slices from WT mice with 100 nM phorbol 12,13-dibutyrate (PDBU) increased pS408/9 immunoreactivity consistent with published studies demonstrating that both residues are substrates of PKC (8). In contrast, pS408/9 immunoreactivity was not detected in S408/9A mice. (*B*) Biotinylation revealed that the surface levels of the β3 subunits, along with the synaptic α2 subunits, were increased in the S408/9A mice, whereas surface accumulation of $GABA_A$Rs containing α4 subunits was decreased. Hippocampal slices were subjected to biotinylation, followed by immunoblotting with anti-α2, anti-α4, and anti-β3 subunit antibodies. The ratio of surface/total (S/T%WT) was measured in S408/9A mice and WT control mice, and values were then normalized to WT controls (100%, red line). Total expression levels were also compared between genotypes (T%WT). *Significantly different from control ($P < 0.05$, *t* test; $n = 5$–6 mice of each genotype). (*C*) Forty-micron hippocampal slices were stained with antibodies against the α2 and α4 subunits and gephyrin fluorescent-conjugated secondary antibodies, followed by confocal microscopy. The number of α2/gephyrin-positive puncta and α4 puncta was then compared within the dentate gyrus between genotypes. Preventing phosphorylation of the β3 subunit increases the number of inhibitory synapses in the dentate gyrus of the hippocampus but reduces α4 puncta immunoreactivity. *Significantly different from control ($P < 0.001$, *t* test; $n = 3$ mice of each genotype). (Scale bars: 10 μm.)

contrast, the α4 subunit was decreased to 81.0 ± 4.5% of levels seen in WT ($P < 0.05$, $n = 6$ mice of each genotype; Fig. 1*B*). These changes in cell surface accumulation were mirrored by parallel changes in increased total expression levels of the α2 subunits and decreased total expression levels of the α4 subunits to 120.7 ± 4.3% and 85.3 ± 7.0%, respectively, compared with WT controls ($P < 0.05$, $n = 4$–8 mice of each genotype; Fig. 1*B*).

To characterize the subcellular distribution of $GABA_A$Rs in S408/9A mice, hippocampal sections were subjected to immunohistochemistry with antibodies against $GABA_A$R α2 or α4 subunits. In some experiments, sections were also stained with antibodies against the inhibitory scaffold protein gephyrin. Sections were then visualized using confocal microscopy, and subunit expression levels were quantified within the dentate gyrus. The number of inhibitory synapses defined as α2/gephyrin puncta were increased in S408/9A mice compared with WT littermates (23.4 ± 2.5 vs. 32.0 ± 0.6 for WT and S408/9A mice, respectively; $P < 0.05$, $n = 3$ mice of each genotype; Fig. 1*C*). In contrast, the number of puncta of α4 subunit immunoreactivity was decreased (13.1 ± 1.2 vs. to 37.4 ± 0.8 puncta per 2,500 μm^2 for S408/9A and WT mice, respectively; $P < 0.001$; Fig. 1*C*). Additionally, in contrast to the effects seen with $GABA_A$Rs, the levels of gephyrin, postsynaptic density protein-95, and the AMPA receptor subunit GluA1 were unaffected by the S408/9A mutation (Fig. S2).

Collectively, these results reveal that S408/9A mice have deficits in the cell surface accumulation of $GABA_A$Rs that mediate tonic inhibition but an increased level of those $GABA_A$Rs that mediate phasic inhibition.

S408/9A exhibited an increase in phasic inhibition and decreased tonic current. To examine the functional significance of the alterations in $GABA_A$R expression seen in S408/9A mice, we used patch-clamp recording to analyze GABAergic inhibition in dentate gyrus granule cells (DGGCs). In DGGCs from S408/9A mice, tonic current was significantly decreased (24.7 ± 4.1 vs. 11.9 ± 2.2 pA for WT and S408/9A mice, respectively; $P < 0.005$, $n = 10$–11 cells, three mice of each genotype; Fig. 2*A*). In contrast, the amplitude of spontaneous inhibitory postsynaptic currents (sIPSCs) was significantly increased in S408/9A mice compared with WT controls (28.4 ± 2.4 vs. 42.5 ± 3.3 pA for WT and S408/9A mice, respectively; $P < 0.005$, $n = 17$–18 cells, three mice of each genotype; Fig. 2*B*). However, the frequency (4.5 ± 0.2 vs. 4.4 ± 0.1 Hz for WT and S408/9A mice, respectively) and decay time (44.7 ± 12.8 vs. 24.8 ± 2.5 ms for WT and S408/9A mice, respectively; $P > 0.05$, $n = 17$–18 cells, three mice of each genotype) of sIPSCs was comparable between genotypes.

We also assessed the impact of the modifications in GABAergic inhibition on neuronal excitability. First, we compared the properties of excitatory postsynaptic currents (EPSCs) in DGGCs. In S408/9A mice, EPSC amplitude was significantly increased (14.6 ± 1.05 vs. 18 ± 1.02 pA for WT and S408/9A mice, respectively; $P < 0.05$; Fig. 2*C*) with no difference in frequency (1.4 ± 0.3 vs. 1.3 ± 0.2 Hz for WT and S408/9A mice, respectively). Moreover, their decay was also prolonged (2.1 ± 0.1 vs. 2.4 ± 0.2 ms for WT and S408/9A mice, respectively; $P < 0.05$, $n =$ 14–16 cells, three mice of each genotype). However, net excitability of DGGCs and their resting membrane potentials were not modified by the S408/9A mutation ($n = 19$–20 cells, three mice of each genotype; Fig. 2*D* and Table S1).

Therefore, S408/9A mice have reduced tonic but enhanced phasic inhibition, but these changes do not lead to any gross changes in neuronal excitability, presumably because S408/9A mice also exhibit elevations in EPSC amplitude.

S408/9A Mice Exhibit Deficits in Social Interaction and Increased Repetitive Behavior. ASDs have a common core of behavioral deficits, including reduced social interaction and increased repetitive behavior. Therefore, we assessed if any of these parameters are altered in S408/9A mice. First, we assessed if the respective mutation modifies motor coordination as measured using the rotarod, a critical control for data interpretation in rodent behavioral experiments. The latency to fall in the rotarod test was not different at 16–32 rpm in S408/9A mice compared with WT mice (Fig. S3*A*). Likewise, there were no differences between genotypes for the total distance traveled or dwell time in the center of the open field (Fig. S3 *B* and *C*). We also compared anxiety-like behavior using the light/dark test. WT and S408/9A mice spent equivalent time in the light chamber (46.9 ± 2.2% vs. 41.8 ± 2.5% for WT and S408/9A mice, respectively; $P > 0.05$, $n = 12$ mice of each genotype; Fig. S3*D*).

Social behavior was measured using the two-choice and three-chamber social interaction test. In the two-choice assay, WT controls spent more time in the chamber containing the novel mouse than in the chamber containing the empty cage, whereas S408/9A mice had no preference for the novel mouse over the

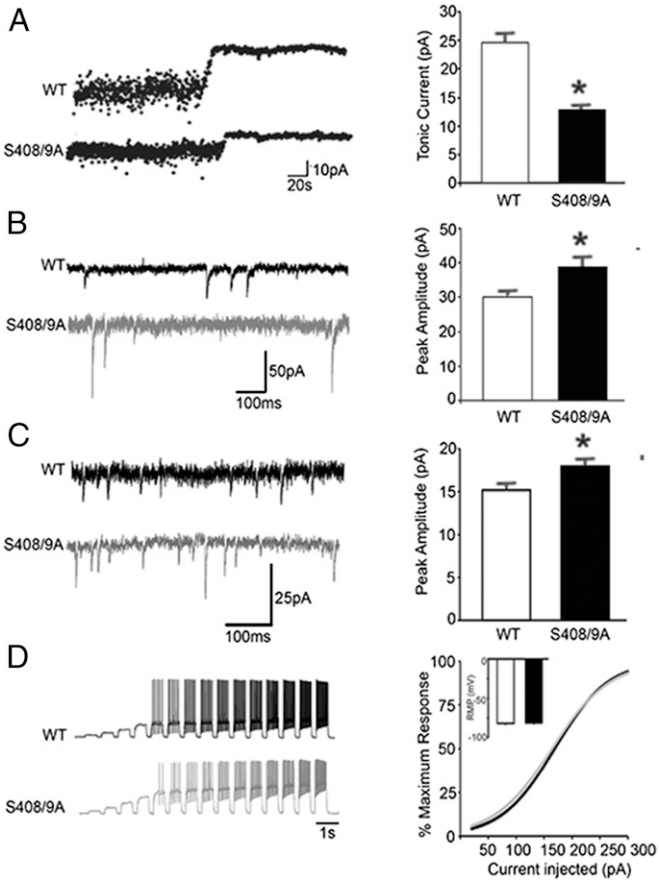

Fig. 2. Characterization of phasic and tonic inhibition in S408/9A mice. (*A*) Tonic conduction is decreased in S408/9A mice. Tonic current in DGGCs was compared between genotypes in the presence and absence of gabazine. The tonic current amplitude of S408/9A mice was significantly smaller than tonic current amplitude of WT mice. *Significantly different from control ($P < 0.01$, *t* test; $n = 10$–11 cells, three mice of each genotype). (*B*) sIPSCs were recorded from DGGCs of WT mice (black) and S408/9A mice (gray) *Significantly different from WT control ($P < 0.001$, *t* test; $n = 17$–18 cells, three mice of each genotype). (*C*) Examples of EPSCs recorded from DGGCs of WT mice (black) and S408/9A mice (gray) *Significantly different from control ($P <$ 0.05, *t* test; $n = 14$–16 cells, three mice of each genotype). (*D*) Representative recordings of action potential firing in DGGCs from WT mice (black) and S408/9A mice (gray) in response to 0.5-s current injections from 20 to 300 pA in 20-pA increments. Average input/output curves from DGGCs from WT mice (black) and S408/9A mice (gray) are shown as a Boltzmann function generated by the averages of the fitted parameters. (*Inset*) No difference in the resting membrane potential (RMP) was observed between genotypes. Values are mean ± SEM ($n = 19$–21 cells, three mice of each genotype).

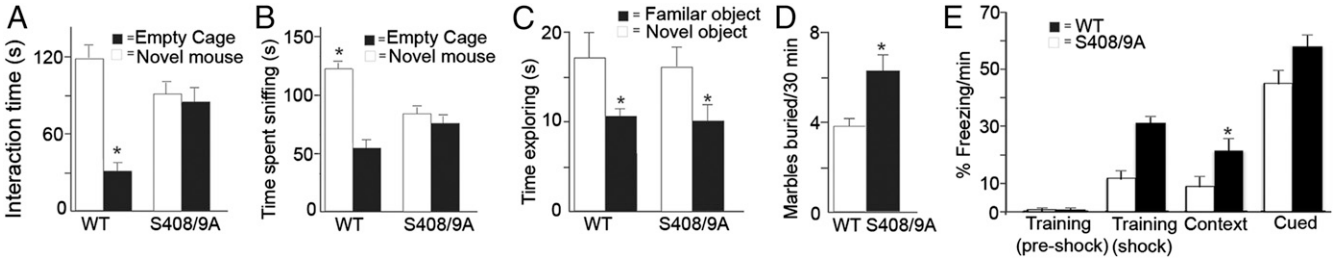

Fig. 3. Characterization of social interaction and repetitive-like behavior in S408/9A mice. (*A*) Preference for an empty cage or novel mouse was determined in a two-choice social interaction setup. *Significantly different from control ($P < 0.01$, ANOVA with Tukey's post hoc comparison; $n = 12$ mice of each genotype). (*B*) Three-chamber social interaction assay was used to measure the preference for a novel mouse or an empty cage. The amount of time mice spent in a predefined sniffing zone around the empty cage or novel mouse was digitally tracked. *Significantly different from control ($P < 0.001$, ANOVA with Tukey's post hoc comparison; $n = 12$–16 mice of each genotype). (*C*) Preference for a familiar object or a novel object was determined for the genotypes. *Significantly different from control ($P < 0.05$, ANOVA with Tukey's post hoc comparison; $n = 10$–12 mice of each genotype). (*D*) Repetitive-like behavior was assessed using the marble burying assay. ($P < 0.01$, *t* test; $n = 18$–19 mice of each genotype). (*E*) Learning and memory were assessed using the fear-conditioning assay. The percentage of freezing per minute was assessed during training and for context-dependent and cued-dependent learning. *Significantly different from control ($P < 0.05$, *t* test; $n = 12$–13 mice of each genotype).

empty cage (time spent interacting with empty cage: 49.8 ± 7.4 s (WT), 86.6 ± 17.6 s (S408/9A); time spent interacting with novel mouse: 119.4 ± 19.0 s (WT), 92.7 ± 17.7 s (S408/9A); $n = 12$ mice of each genotype, $P < 0.01$; Fig. 3*A*). Consistent with the profound deficits in social interaction observed in the two-choice assay, S408/9A mice exhibited no preference for the novel mouse in the three-chamber social interaction assay. WT controls spent more time in the novel mouse sniffing zone than in the empty cage sniffing zone (time spent interacting with empty cage: 55.4 ± 5.8 s (WT), 71.9 ± 8.4 s (S408/9A); time spent interacting with novel mouse: 123.8 ± 5.1 s (WT), 85.7 ± 6.9 s (S408/9A); $n = 12$–16 mice of each genotype, $P < 0.01$; Fig. 3*B*). In contrast, S408/9A mice showed no preference for the novel mouse over an empty cage, consistent with ASD-like deficits in social interaction. As a control for our measurements for social preference, we examined the ability of S408/9A mice to discriminate between a novel object and a familiar object. Both WT controls and S408/9A mice spent more time interacting with the novel object (66 ± 0.9% vs. 64 ± 7.7% of total time for WT and S408/9A mice, respectively; $P < 0.05$, $n = 10$–11 mice of each genotype; Fig. 3*C*).

To measure repetitive-like behavior in S408/9A mice, we used the marble burying assay. S408/9A mice displayed an increase in repetitive-like behavior in the marble burying test (6.0 ± 0.6 marbles in 30 min compared with 3.8 ± 0.5 marbles in WT controls; $P < 0.001$, $n = 18$–19 mice of each genotype; Fig. 3*D*). Therefore, S408/9A mice exhibited an increase in repetitive-like behavior and deficits in social interaction, which are behavioral characteristics commonly observed in ASDs.

Finally, we assessed if the S408/9A mutation has an impact on cognition by comparing contextual and cued fear conditioning between genotypes. S408/9A mice exhibited enhanced context-dependent learning (training: 11.8 ± 3.0% freezing per minute (WT), 32.1 ± 4.3% freezing per minute (S408/9A); $P > 0.05$; context: 8.9 ± 3.4% freezing per minute (WT), 21.4 ± 4.2% freezing per minute (S408/9A); $P < 0.05$; Fig. 3*E*) compared with WT controls but no statistical differences in cue-dependent learning (cued: 45.1 ± 6.6% freezing per minute (WT), 60.8 ± 6.4% freezing per minute (S408/9A); $P > 0.05$; Fig. 3*E*).

S408/9A Mice Have Increased Seizure Susceptibility. ASDs are frequently comorbid with epilepsy. Therefore, we analyzed the impact of the S408/9A mutation on seizure susceptibility. Mice were implanted with EEG electrodes, and seizures were induced with 20 mg/kg of kainic acid and monitored to ensure seizures reached stage 3–4 on the Racine scale (forelimb clonus and rearing with forelimb clonus). Representative EEG traces during epileptiform events captured 30 min after kainic acid injection illustrate a marked increase in epileptiform activity in S408/9A mice over WT controls (Fig. 4*A*). Strikingly, S408/9A mice exhibited a faster onset to the first epileptiform event compared with WT mice (4.6 ± 0.7 vs. 11.2 ± 1.1 min of latency for S408/9A and WT mice, respectively; $P < 0.001$, $n = 8$–10 mice of each genotype; Fig. 4*B*). Additionally, S408/9A mice entered status epilepticus at an earlier time point than WT controls (41.8 ± 4.3 vs. 61.5 ± 8.6 min for S408/9A and WT mice, respectively; $P < 0.05$, $n = 8$–10 mice of each genotype; Fig. 4*B*). Furthermore, S408/9A mice spent a greater percentage of the total time experiencing epileptiform activity compared with WT controls (82.5 ± 2.1% vs. 65.4 ± 6.4% for S408/9A and WT mice, respectively; $P < 0.05$, $n = 8$–10 mice of each genotype; Fig. 4*B*). Therefore, the S408/9A mutation significantly increases seizure susceptibility.

S408/9A Mice Exhibited Increased Hippocampal Dendritic Spine Density. Alterations in spine structure are a common feature in ASDs (17). Therefore, we assessed if the alterations in GABAergic inhibition have an impact on dendritic structure. Brains from both genotypes were subjected to Golgi staining and visualized using stereology. We quantified the density of spines along 30-μm-long sections of

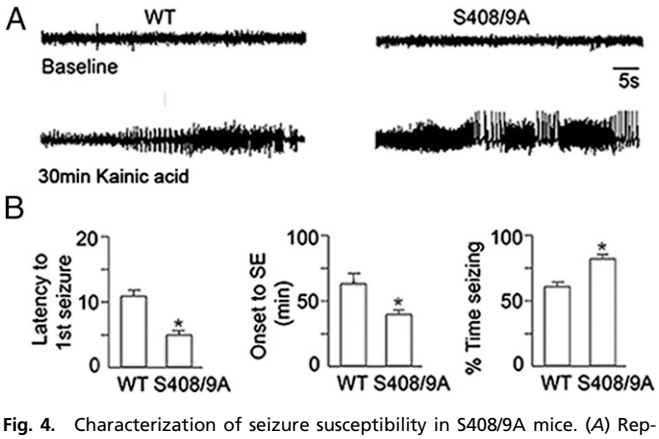

Fig. 4. Characterization of seizure susceptibility in S408/9A mice. (*A*) Representative EEG traces for WT and S408/9A mice at baseline and 30 min after kainic acid injection. (*B*) Latency to the first epileptiform activity, onset of status epilepticus (SE), and total time experiencing epileptiform activity were digitally tracked and measured. S408/9A mice had a shorter latency to the first epileptiform activity, faster onset of status epilepticus, and spent a great percentage of time experiencing epileptiform activity compared with WT controls. *Significantly different from control ($P < 0.05$, *t* test; $n = 8$–10 mice of each genotype).

dendrites in the molecular layer above the dentate gyrus of the hippocampus. In S408/9A mice, a pronounced increase in spine density was seen (28.6 ± 0.7 vs. 34.8 ± 1.0 per 30-μm dendrite for WT and S408/9A mice, respectively; $P < 0.0001$, $n = 12$ neurons in three independent experiments; Fig. 5*A*). Similarly, the spines in S408/9A mice appeared to be more filopodia-like in structure compared with their equivalents in WT mice, and some exhibited pronounced branching. Therefore, S408/9A mice displayed similar abnormalities in spine structure to those abnormalities reported in *Fmr1* KO mice and patients with ASDs.

S408/9A Phosphorylation Is Increased in *Fmr1* KO (Fragile X Syndrome) Mice. To assess the relevance of our studies further, we measured S408/9 phosphorylation in *Fmr1* KO mice, a model of Fragile X syndrome (FXS). S408/9 phosphorylation was significantly increased to 285.6 ± 24.3% in *Fmr1* KO mice compared with WT controls ($P < 0.005$; $n = 3$ mice of each genotype; Fig. 5*B*). In contrast to S408/9, phosphorylation of S383 was similar in *Fmr1* KO mice compared with WT controls ($P > 0.05$, $n = 3$ mice of each genotype; Fig. 5*B*).

Discussion

Deficits in the efficacy of neuronal inhibition mediated by $GABA_A$Rs containing the β3 subunit are widely believed to contribute to the pathophysiology of ASDs. Accordingly, modifications in $GABA_A$R β3 subunit gene structure and/or protein expression levels, together with both deletions and duplications of the 15q11–13 locus, are leading causes of ASDs (5, 18).

In vitro studies have shown that phosphorylation of S408/9 regulates the cell surface stability and synaptic accumulation of β3-containing $GABA_A$Rs (7), and, here, we have analyzed the significance of this putative regulatory process for the pathophysiology of ASDs. To do so, we created a S408/9A knock-in mouse using homologous recombination. S408/9A mice were viable and did not exhibit any overt phenotypes or gross alterations in the structure of the hippocampus. Consistent with the lowered affinity for AP2 in the S408/9A mutation in vitro, the cell surface expression levels of the β3 subunit in the hippocampus were increased in S408/9A mice compared with WT controls. Within the dentate gyrus, the β3 subunit assembles with the α2/γ2 or α4/δ subunits to form $GABA_A$R subtypes that mediate phasic and tonic inhibition, respectively (2). Strikingly, in the dentate gyrus of S408/9A mice, there was a significant increase in the expression levels of the α2 subunit and the number of inhibitory synapses. In contrast, deficits in the expression levels of the α4 subunit were seen. Thus, in addition to membrane trafficking, S408/9 and/or their phosphorylation may play a role in regulating the assembly of individual $GABA_A$R subtypes. Significantly, our findings of alterations in α4 and β3 subunit expression are consistent with GABAergic dysfunction in *Mecp2* and *Fmr1* KO mice, which are accepted models of ASDs (11, 19, 20).

Consistent with this result, the amplitude of sIPSCs was increased and their decay was slowed in DGGCs from S408/9A mice. In contrast, a reciprocal decrease in the cell surface accumulation of the α4 subunit was seen in S408/9A mice, which paralleled a reduction in tonic current. The gross excitability of DGGCs as measured by current injection was not altered between strains, reflecting the increase in EPSC amplitude in S408/9A mice. Therefore, preventing the phosphodependent modulation of the $GABA_A$Rs by mutating S408/9 in the β3 subunit to alanines alters the equilibrium between phasic and tonic inhibition in the dentate gyrus.

Previous in vitro studies have suggested that for synaptic $GABA_A$Rs containing α1/2β3γ2 subunits, mutation of S408/9A does not compromise receptor assembly, or transport to the plasma membrane, but selectively reduces their endocytosis (9). Therefore, the increased synaptic accumulation of the α2 subunit in S408/9A mice presumably results from their enhanced residence time on the plasma membrane. In contrast to synaptic receptors, the mechanisms that control the membrane trafficking of receptors containing α4 subunits are less well defined. However, it is evident from our results that phosphorylation of S408/9 may play opposing roles in regulating the assembly and membrane trafficking of α4 subunit containing $GABA_A$Rs to those roles established for subtypes that mediate phasic inhibition. Clearly, further studies are required to identify the role that S408/9 and their phosphorylation plays in regulating the differential membrane trafficking of $GABA_A$R subtypes that mediate phasic and tonic inhibition.

In parallel with these modifications in GABAergic inhibition, the number of dendritic spines was strikingly increased in the mutant mice. Significantly, overexpressing S408/9A cDNA in cultured hippocampal neurons leads to similar changes in spine maturity to those changes seen in S408/9A mice (7). It is emerging that tonic inhibition plays a central role in reducing neuronal excitability, particularly at depolarizing membrane potentials (21). Given the emerging role for tonic inhibition in regulating neuronal output, the deficits in the efficacy of this process in S408/9A mice may lead to prolonged neuronal depolarization and enhanced intracellular Ca^{2+} signaling, which would be predicted to have significant effects on spine architecture.

In addition to modifications in dendritic structure, ASDs have a common core of behavioral symptoms, including increased repetitive behavior and anxiety, together with deficits in social interaction (17). Therefore, we compared these parameters between genotypes. Compared with WT controls, S408/9A mice exhibited decreased social interaction as measured in both the two-choice and three-chamber assays; however, S408/9A mice and WT controls

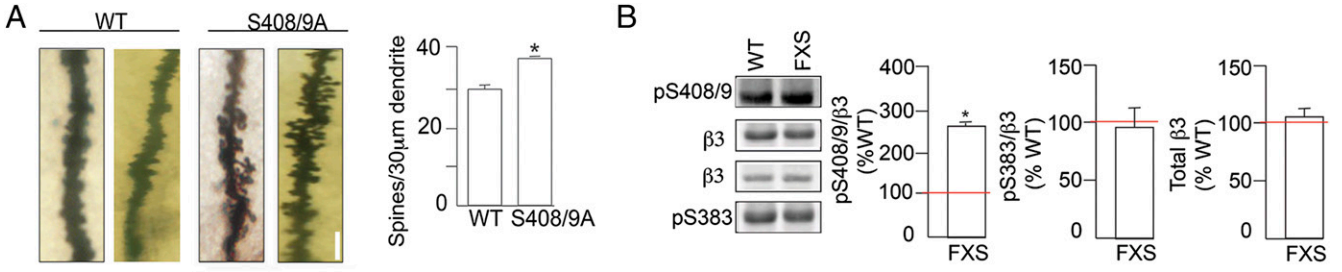

Fig. 5. Characterization of dendritic spine density in DGGCs from S408/9A mice and β3 phosphorylation in *Fmr1* KO (FXS) mice. (*A*) Representative dendrites from DGGCs of two different mice. (Scale bar: 2 μm.) The number of spines per 30 μm of dendrite was then determined and compared between genotypes. *Significantly different from control ($n = 12$ neurons from three independent experiments, three mice of each genotype; $P < 0.0001$, *t* test). (*B*) Hippocampal lysates from WT and *Fmr1* KO mice on a FVB/N (Friend leukemia virus B strain) background were subjected to SDS/PAGE and immunoblotted with pS408/9, pS383, and β3 subunit antibodies. The pS408/9/β3 or pS383/β3 ratios in *Fmr1* KO mice (FXS) were normalized to WT controls (100%; red line). *Significantly different from control ($P < 0.01$, *t* test; $n = 3$ mice of each genotype).

shared a similar preference for a novel object over a familiar object. S408/9A mice also exhibited an increase in repetitive-like behavior as measured using the marble burying assay. Significantly, the mutation did not alter locomotor activity, behavior in the open field, or behavior in the light/dark test. S408/9A mice did not appear to exhibit any modifications in anxiety. ASDs are often comorbid with epilepsy, and consistent with this comorbidity, S408/9A mice exhibit increased sensitivity to kainate-induced seizures. Thus, although the changes in phasic and tonic inhibition seen in S408/9A mice do not appear to lead to changes in net neuronal excitability, they are important determinants of epileptogenesis. Finally, we noted that in the *Fmr1* KO mouse model of FXS, specific alterations in S408/9 phosphorylation were seen. The mechanism linking deficits in FMRP expression and enhanced S408/9 phosphorylation requires further experimentation. However, it is interesting to note that FMRP is part of a signaling complex that contains protein phosphatase 2A (PP2A), the principle phosphatase that dephosphorylates S408/9 (10, 22, 23). Thus, deficits in FMRP expression levels may affect the stability and/or subcellular targeting of PP2A, leading to reduced rates of S408/9 dephosphorylation.

In conclusion, our results suggest that alterations in the phosphorylation status of $GABA_AR$ β3 resulting in compromised GABAergic inhibition are central to the pathophysiology of FXS. Therefore, restoring the efficacy of tonic inhibition may be a useful therapeutic strategy to alleviate the burdens of ASDs.

Materials and Methods

All protocols were approved by Tufts University's Institutional Animal Care and Use Committee and were conducted in accordance with the NIH *Guide for the Care and Use of Laboratory Animals* (24). More detailed information on materials and methods is provided in *SI Materials and Methods*.

Creation of the S408/9A Mice. The S408/9A mice were created using homologous recombination as detailed previously (25).

Biochemical Measurements. Antibodies used in this study have been described previously, as have the methods for immunoblotting and immunoprecipitation (22, 26).

Electrophysiology and EEG Recordings. Phasic and tonic inhibition was measured using the patch-clamp technique (27). The Pinnacle Technology system and LabChart (ADInstruments) were used for EEG recordings and analysis as previously described (28).

Behavior. Measurements using the rotarod and activity in the open field and anxiety were assessed as described previously (26).

ACKNOWLEDGMENTS. We thank Jay Boltax and Hew Mun Lau (McLean Hospital) for technical assistance in generating the mutant allele in ES cells. This work was supported by Grant 206026 from the Simons Foundation (to S.J.M.); NIH–National Institute of Neurological Disorders and Stroke Grants NS051195, NS056359, NS081735, R21NS080064, and NS087662 (to S.J.M.); NIH–National Institute of Mental Health Grant MH097446 (to P.A.D. and S.J.M.); and US Department of Defense Grant AR140209 (to P.A.D. and S.J.M.). J.M. is supported by Grant NS073574, and U.R. is supported by Grant R01MH080006.

1. Rudolph U, Möhler H (2006) GABA-based therapeutic approaches: GABAA receptor subtype functions. *Curr Opin Pharmacol* 6(1):18–23.
2. Brickley SG, Mody I (2012) Extrasynaptic GABA(A) receptors: Their function in the CNS and implications for disease. *Neuron* 73(1):23–34.
3. DeLorey TM, et al. (1998) Mice lacking the beta3 subunit of the GABAA receptor have the epilepsy phenotype and many of the behavioral characteristics of Angelman syndrome. *J Neurosci* 18(20):8505–8514.
4. Abrahams BS, Geschwind DH (2008) Advances in autism genetics: On the threshold of a new neurobiology. *Nat Rev Genet* 9(5):341–355.
5. Delahanty RJ, et al. (2011) Maternal transmission of a rare GABRB3 signal peptide variant is associated with autism. *Mol Psychiatry* 16(1):86–96.
6. Brandon NJ, et al. (1999) Synaptic targeting and regulation of GABA(A) receptors. *Biochem Soc Trans* 27(4):527–530.
7. Jacob TC, et al. (2009) GABA(A) receptor membrane trafficking regulates spine maturity. *Proc Natl Acad Sci USA* 106(30):12500–12505.
8. Nakamura Y, Darnieder LM, Deeb TZ, Moss SJ (2015) Regulation of GABAARs by phosphorylation. *Adv Pharmacol* 72:97–146.
9. Kittler JT, et al. (2005) Phospho-dependent binding of the clathrin AP2 adaptor complex to GABAA receptors regulates the efficacy of inhibitory synaptic transmission. *Proc Natl Acad Sci USA* 102(41):14871–14876.
10. Terunuma M, et al. (2008) Deficits in phosphorylation of GABA(A) receptors by intimately associated protein kinase C activity underlie compromised synaptic inhibition during status epilepticus. *J Neurosci* 28(2):376–384.
11. Martin BS, Corbin JG, Huntsman MM (2014) Deficient tonic GABAergic conductance and synaptic balance in the fragile X syndrome amygdala. *J Neurophysiol* 112(4):890–902.
12. DeLorey TM (2005) GABRB3 gene deficient mice: A potential model of autism spectrum disorder. *Int Rev Neurobiol* 71:359–382.
13. Jacob TC, Moss SJ, Jurd R (2008) GABA(A) receptor trafficking and its role in the dynamic modulation of neuronal inhibition. *Nat Rev Neurosci* 9(5):331–343.
14. Smith KR, et al. (2012) Stabilization of GABA(A) receptors at endocytic zones is mediated by an AP2 binding motif within the GABA(A) receptor β3 subunit. *J Neurosci* 32(7):2485–2498.
15. Moss SJ, Doherty CA, Huganir RL (1992) Identification of the cAMP-dependent protein kinase and protein kinase C phosphorylation sites within the major intracellular domains of the beta 1, gamma 2S, and gamma 2L subunits of the gamma-aminobutyric acid type A receptor. *J Biol Chem* 267(20):14470–14476.
16. Jurd R, Tretter V, Walker J, Brandon NJ, Moss SJ (2010) Fyn kinase contributes to tyrosine phosphorylation of the GABA(A) receptor gamma2 subunit. *Mol Cell Neurosci* 44(2):129–134.
17. Hutsler JJ, Zhang H (2010) Increased dendritic spine densities on cortical projection neurons in autism spectrum disorders. *Brain Res* 1309:83–94.
18. Kang JQ, Barnes G (2013) A common susceptibility factor of both autism and epilepsy: Functional deficiency of GABA A receptors. *J Autism Dev Disord* 43(1):68–79.
19. Olmos-Serrano JL, et al. (2010) Defective GABAergic neurotransmission and pharmacological rescue of neuronal hyperexcitability in the amygdala in a mouse model of fragile X syndrome. *J Neurosci* 30(29):9929–9938.
20. Chao HT, et al. (2010) Dysfunction in GABA signalling mediates autism-like stereotypies and Rett syndrome phenotypes. *Nature* 468(7321):263–269.
21. Wlodarczyk AI, et al. (2013) Tonic GABAA conductance decreases membrane time constant and increases EPSP-spike precision in hippocampal pyramidal neurons. *Front Neural Circuits* 7:205.
22. Jovanovic JN, Thomas P, Kittler JT, Smart TG, Moss SJ (2004) Brain-derived neurotrophic factor modulates fast synaptic inhibition by regulating GABA(A) receptor phosphorylation, activity, and cell-surface stability. *J Neurosci* 24(2):522–530.
23. Narayanan U, et al. (2007) FMRP phosphorylation reveals an immediate-early signaling pathway triggered by group I mGluR and mediated by PP2A. *J Neurosci* 27(52):14349–14357.
24. Committee on Care and Use of Laboratory Animals (1996) *Guide for the Care and Use of Laboratory Animals* (Natl Inst Health, Bethesda), DHHS Publ No (NIH) 85-23.
25. Terunuma M, et al. (2014) Postsynaptic GABAB receptor activity regulates excitatory neuronal architecture and spatial memory. *J Neurosci* 34(3):804–816.
26. Tretter V, et al. (2009) Deficits in spatial memory correlate with modified gamma-aminobutyric acid type A receptor tyrosine phosphorylation in the hippocampus. *Proc Natl Acad Sci USA* 106(47):20039–20044.
27. Kretschmannova K, et al. (2013) Enhanced tonic inhibition influences the hypnotic and amnestic actions of the intravenous anesthetics etomidate and propofol. *J Neurosci* 33(17):7264–7273.
28. Lee V, Maguire J (2013) Impact of inhibitory constraint of interneurons on neuronal excitability. *J Neurophysiol* 110(11):2520–2535.

Supporting Information

Vien et al. 10.1073/pnas.1514657112

SI Materials and Methods

Mice. Ten- to 12-wk-old male S408/9A mice and the corresponding WT littermates were housed in a 12-h light/dark cycle with standard rodent food and water ad libitum. For behavioral testing, animals were acclimatized to the testing room for 1 h before the start of all procedures.

***Gabrb3* (Gene That Encodes for the β3 $GABA_AR$ Subunit Protein).** S408/9A mice were generated by gene targeting in murine ES cells using standard techniques. Briefly, a targeting vector was constructed containing 7.4 kb of homologous genomic sequence (from 3 kb upstream of the 5′ end of exon 9 to 4.4 kb downstream of the 5′ end of exon 9). The genomic DNA was subcloned from a substrain 129S5 BAC, obtained from the Wellcome Trust Sanger Institute. In exon 9 (the final exon), the codons for S408/9 of the $GABA_AR$ β3 subunit were mutated to alanine codons (S408/9A). A *lox*P-flanked neomycin expression cassette (*lox*P-FRT-PGKneobpA-FRT-SA-4xSv40pA-SD-*lox*P) was inserted 0.3 kb upstream of the 5′ end of exon 9. An HSV-TK (herpes simplex virus-thymidine kinase) cassette for negative selection was positioned 3′ of the homology. The NotI-linearized targeting vector was electroporated into TC-1 ES cells (derived from substrain 129S6, a gift from Phil Leder, Department of Genetics, Harvard Medical School, Belmont, MA). Correctly targeted clones were identified by PCR and sequenced to verify the double-point mutation and the loxP sites, and they were injected into C57BL/6J mouse blastocysts. Chimeric male mice were bred with WT C57BL/6J females, and the entire neomycin expression cassette was excised by Cre/*lox*P-mediated recombination. Mice were backcrossed to C57BL/6J for a minimum of 10 generations. Experimental animals were derived from heterozygous breedings. The proposed allele symbol for the β3-S408/9A allele in the MGI database is $Gabrb3^{tm2Uru}$.

Antibodies. Polyclonal rabbit antibodies against α2, α4, β2, and δ were gifts from Verena Tretter and Werner Sieghart (both from Medical University Vienna, Vienna). Anti-β3 and anti–phospho-β3 (phospho-S408/9 and phospho-S383) antibodies were generated and verified by the S.J.M. laboratory (9, 10, 12). The following antibodies were purchased from commercial vendors: monoclonal anti-α1 (clone N95/35; NeuroMab), monoclonal anti-gephyrin (catalog no. 147011; Synaptic Systems), and monoclonal anti-actin (catalog no. A2228; Sigma–Aldrich).

Western Blot. Standard Western blotting protocols were used as previously described (10). Briefly, hippocampi were rapidly dissected, flash-frozen, and lysed in lysis buffer composed of the following: 20 mM Tris·HCl (pH 8.0), 150 mM NaCl, 1% Triton X-100, 5 mM EDTA, 10 mM NaF, 2 mM Na_3VO_4, 10 mM pyrophosphate, 0.1% SDS, and 50 mM NaF. Total protein concentration was established, and 40 μg of hippocampal lysate was subjected to SDS/PAGE, transferred to nitrocellulose membranes, and blocked with 5% (wt/vol) BSA in Tris-buffered saline-Tween 20 for 1 h. Membranes were immunoblotted with the indicated primary antibodies, and following extensive rinsing, they were probed with HRP-conjugated secondary antibodies and detected with enhanced chemiluminescence. Blots were imaged, and data were normalized to actin and quantified with the CCD-based LAS 3000 system (FujiFilm).

Surface Biotinylation. Three hundred fifty-micron-thick hippocampal slices from 10- to 12-wk-old male WT control (C57BL/6) mice or age-matched male S408/9A mice were prepared on a vibratome (Leica VT1000S) in cold, oxygenated artificial cerebral spinal fluid (ACSF) composed of 124 mM NaCl, 3 mM KCl, 25 mM $NaHCO_3$, 2 mM $MgSO_4$, 2 mM $CaCl_2$, 1.1 mM NaH_2PO_4, and 10 mM glucose (pH 7.4). After sectioning, slices were allowed a 1-h recovery period in oxygenated, ice-cold ACSF. Following the recovery period, slices were incubated for 30 min at 4 °C with 1 mg/mL NHS-SS-biotin (Pierce). Following three rinses in ice-cold ACSF to remove excess biotin, hippocampal samples were lysed. After adjusting for protein concentration, hippocampal lysates were incubated with streptavidin beads (Pierce) overnight at 4 °C. Bound substances were subjected to SDS/PAGE, followed by immunoblotting with the indicated antibodies. Immunoblots were quantified using the CCD-based LAS 3000 system. For phospho-specific antibodies, the ratio of phospho-β3/total-β3 was calculated and S408/9A values were normalized to WT control (100%).

EEG Recordings. EEGs were performed as previously described (28). Age-matched male littermates, aged 10–12 wk, were used for recording EEGs in awake, behaving animals. Mice were deeply anesthetized and implanted with prefabricated head mounts containing six-pin connectors with two electromyogram reference electrodes (Pinnacle Technology) 2.0 mm posterior to the bregma, along the midsagittal suture, and 2 mm below the dura. Following a 1-wk recovery period, EEG activity was monitored using the Pinnacle Technology turnkey system with a 100× amplifier and were high-pass-filtered at 1.0 Hz (PowerLabs; ADInstruments). A 30-min baseline was obtained before an i.p. injection of 20 $mg{\cdot}kg^{-1}$ kainic acid (Tocris), followed by continuous EEG monitoring for an additional 120 min. Epileptiform activity was defined as electrographic events with amplitudes greater than twofold the standard deviation of the averaged baseline that last a minimum of 10 s and are separated from another event by greater than 10 s. Epileptiform activity was additionally confirmed by an increase in the power and frequency of high-amplitude events. Latency to the first seizure was defined as the time from injection of kainic acid until the first electrographic seizure. Duration of epileptiform activity was calculated from the cumulative time in minutes of epileptiform activity divided by 120 min. The onset of status epilepticus was defined as epileptiform activity lasting longer than 5 min with no silent period greater than 10 s. Duration of epileptiform activity, latency to the first epileptiform event, and latency to onset of status epilepticus were quantified using LabChart, version 7 (ADInstruments).

Immunohistochemistry. Ten- to 12-wk-old male mice were perfused intracardially with 4% (wt/vol) paraformaldehyde, brains were dissected and immersed in 30% (wt/vol) sucrose for 72 h, and 40-μm-thick sections were prepared from fresh-frozen tissue using a microtome. Free-floating sections were processed for immunohistochemistry. Tissue was extensively rinsed in BupH-PBS (Thermo Fisher Scientific) and blocked for 1 h in 10% (wt/vol) BSA with 0.3% Triton X-100 in BupH-PBS. Tissue was incubated overnight at room temperature with the indicated antibodies, extensively rinsed in BupH-PBS, and incubated for 2 h in Alexa Fluor 488 and/or Alexa Fluor 568 secondary antibodies (Life Technologies, Thermo Fisher Scientific). After extensive rinsing with BupH-PBS, tissues were mounted, dried, and coverslipped with ProLong Gold anti-fade reagent with DAPI (Invitrogen). Images were obtained with a Nikon Ti microscope and analyzed with

ImageJ (NIH) software. Controls consisted of incubating slices in the absence of primary antibody.

Electrophysiology. The brains of male mice were rapidly dissected and placed in oxygenated, ice-cold ACSF solution containing 225 mM sucrose, 2.95 mM KCl, 1.25 mM NaH_2PO_4, 26 mM $NaHCO_3$, 0.5 mM $CaCl_2$, 10 mM $MgSO_4$, 10 mM D-glucose, and 3 mM kynurenic acid and were bubbled with 95% O_2/5% CO_2 (330–340 mosmol^{-1}). Coronal (350-μm-thick) slices were cut using a vibratome. The slices were then incubated at −33 °C in ACSF containing 126 mM NaCl, 2.5 mM KCl, 26 mM $NaHCO_3$, 1.25 mM NaH_2PO_4, 2 mM $CaCl_2$, 10 mM D-glucose, and 2 mM $MgCl_2$ saturated with 95% O_2/5% CO_2 (pH 7.4, 300–310 mosmol^{-1}) for a minimum of 1 h before experimentation. Hippocampal slices were viewed on a fixed-stage upright microscope (Nikon FN-1) with a 40× water immersion objective equipped with differential interference contrast/infrared (DIC/IR) optics. Slices were maintained at 32 °C and gravity-superfused with ACSF solution throughout experimentation. For current-clamp recordings in S408/9A mice, slices were incubated in ACSF in the absence of kynurenic acid. Input/output curves were produced as previously described from DGGCs (28). Briefly, visually identified DGGCs were injected with 0.5-s square wave current injections from 20 to 300 pA in 20-pA increments.

For voltage-clamp recordings, the internal pipette solution contained 140 mM CsCl, 1 mM $MgCl_2$, 0.1 mM EGTA, 10 mM Hepes, 2 mM Mg-ATP, 4 mM NaCl, and 0.3 mM Na-GTP (pH 7.25, 280–290 mosM). Series resistance and whole-cell capacitance were continually monitored throughout the experiment. After these parameters had stabilized for a minimum of 5 min, synaptic currents were recorded using an Axopatch 200B amplifier (Molecular Devices), filtered at 2 kHz, sampled at 20 kHz, digitized (Digidata 1320A; Molecular Devices), and stored for off-line analysis (Minianalysis; Synaptosoft, Inc.). Access resistance of 10–20 MΩ (~80% compensation) was monitored using a voltage step of −5 mV, and data from cells were discarded when >20% change occurred.

sIPSCs were analyzed using pClamp 9.2 (Clampfit; Axon Instruments) and MiniAnalysis software using pooled population data expressed as the mean ± SEM. The decay phase was fitted with a monoexponential function (τ decay), and rise time was analyzed by comparing the mean with 10–90% rise time. Tonic current was calculated as the difference between the holding current before and after application of the indicated $GABA_AR$ antagonist (≥200 μM SR95531 or 100 μM picrotoxin). The mean holding current of a 10-ms epoch was sampled every 100 ms for a single data point, and a Gaussian fit was applied to the resulting all-points histogram. Epochs containing synaptic events or an unstable baseline were excluded from the analysis. Input/output curves were fitted with a Boltzmann function: $f(W) = \text{Max}/(1 + \exp[(I - I_{50})/k])$, where Max = maximum response, k = slope, and I_{50} = amplitude of current that produces 50% of the maximum response.

Fear Conditioning. Fear conditioning was carried out in a single chamber with foot-shock bars. For conditioning and context testing, the chamber walls were covered with patterned panels. The conditioning procedures were a 180-s baseline period, followed by two trials separated by 120-s intervals. For each trial, a 15-s 70-dB tone was played, which terminated with the application of a 1.5-mA foot shock during the last 1 s. Twenty-four hours later, context-dependent memory was assessed by placing the mice in the chambers containing the patterned panels (conditioning environment). The amount of time the mice spent freezing during the trials was digitally tracked and analyzed. Two hours after context testing, cue-dependent memory was assessed by placing the mouse in a chamber without the patterned panels and measuring the amount of time it spent freezing during a 120-s baseline period, followed by two 70-dB tones played for 15 s separated from one another by 60-s intervals.

Open-Field Test. Following a thorough cleaning of the arena with 70% (vol/vol) ethanol, individual mice were placed in the center of a 40 × 40-cm arena and movement was digitally tracked (EthoVision XT 7.0; Noldus Technology). Time spent in a predefined center arena and total distance traveled were calculated.

Light/Dark Box Assay. Following a thorough cleaning with 70% (vol/vol) ethanol of the two equally sized chambers (each chamber is 21 × 21 cm), individual mice were placed in the dark chamber and allowed to roam freely between the dark and light chambers. Movement and time spent in the different chambers were digitally tracked and calculated (EthoVision XT 7.0).

Marble Burying. Mice were transferred into a new cage with 6-inch deep bedding, and 20 glass marbles were placed evenly spaced apart in a 4 × 5 pattern on its surface. Mice were individually placed in the cage, and the number of marbles buried to two-thirds of their depth after 30 min was counted.

Two-Choice Social Assay. In the two-choice assay, the subject mouse is placed at the bottom of a T-shaped container made of Plexiglas with two perpendicular arms (the long arm is 63.5 × 10 cm, and each short arm is 55 × 10 cm, surrounded by 32-cm high walls). All chambers and wire cups were cleaned with 70% (vol/vol) ethanol between each subject mice. The first session is a habituation period, where the subject mouse was able to roam freely across the three arms. This session was followed by a testing session, where a novel object (empty cup) was placed in the left arm or a novel mouse (stranger mouse under the wire cup) was placed in the right arm. The subject mouse was able to move freely across all three arms, and the cumulative time spent in the left arm or right arm was digitally tracked and quantified (EthoVision XT 7.1; Noldus Technology).

Social Novelty. Briefly, on the first day of training, mice were exposed to the open-field arena (40 × 40 cm) for 10 min. On the second day of training, mice were placed in an empty open-field arena for 5 min, followed by 5 min of exposure to two empty cages. On the third day, testing for social novelty was carried out by placing the subject mouse in an empty open-field arena for 5 min, followed by another 5 min when an empty cage (familiar object) or a novel object (empty salt shaker) was placed in opposite corners of the open-field arena. The amount of time the mice spent exploring in a predefined zone around the objects was digitally tracked (EthoVision XT 7.0).

Three-Chamber Social Test. Briefly, we constructed a three-chamber apparatus with Plexiglas containing three equally sized chambers (30 × 30 cm); two doors that can be remotely opened separate the middle chamber from the left and right chambers. A wire cup (4-inch diameter; item no. 010591315704, organizeit.com) was used as the empty cage or housed a stranger mouse (novel mouse), and the sniff zone 5 cm from the center of the wire cup was predefined. All chambers and wire cups were cleaned with 70% (vol/vol) ethanol between subject mice. A 10-min habituation period where the subject mouse was placed in the center chamber with the doors to the other chambers closed was followed by another 10-min session where the subject mouse was able to roam freely across all three chambers. These sessions were followed by a third 10-min session where a novel object (empty cup) was placed in the left chamber or a novel mouse (stranger mouse under the wire cup) was placed in the right chamber. The subject mouse was freely able to move across all three chambers, and the amount of time it spent in the predefined sniff zone (5-cm radius proximal to each cage) was

digitally monitored (EthoVision XT 7.1). A fourth 10-min session was used to test for social novelty, where a second stranger mouse was placed in the previously empty cage. The subject mouse was then able to roam freely across all three chambers, with the right chamber holding the previously encountered mouse (familiar mouse) and the left chamber holding the novel mouse (stranger mouse). Cumulative time spent in the left or right sniffing zone was digitally tracked and quantified. (EthoVision XT 7.1).

Golgi Staining. For Golgi staining, we used the protocol recommended by the manufacturer of the FD Rapid GolgiStain Kit (FD NeuroTechnologies, Inc.). Briefly, mice were deeply anesthetized, and brains were rapidly extracted and rinsed in Milli-Q water generated at Tufts University within the S.J.M. laboratory. Brains were immersed in the provided solutions for 14 d at room temperature in the dark. Following Golgi–Cox immersion, 200-μm-thick coronal sections were prepared on a vibratome. Sections were then developed according to the manufacturer's protocol and dehydrated in 50%, 75%, 95%, and absolute ethanol; cleared in xylene; and coverslipped with Permount (catalog no. SP15; Thermo Fisher Scientific). Dendritic spine analysis was performed on dendritic spines located immediately adjacent to the DGGC layer in the molecular layer of the hippocampus using images collected with a 60× objective (Nikon). Spine density in 30-μm-long sections was calculated.

Statistical Analysis. All data are presented as the mean ± SEM and were analyzed with the Student's *t* test, one-way ANOVA with Turkey's multiple comparison test, and two-way ANOVA with Bonferroni's post hoc comparison. Unless otherwise indicated, $P < 0.05$ was considered statistically significant. All analyses were done using Prism 6 (GraphPad).

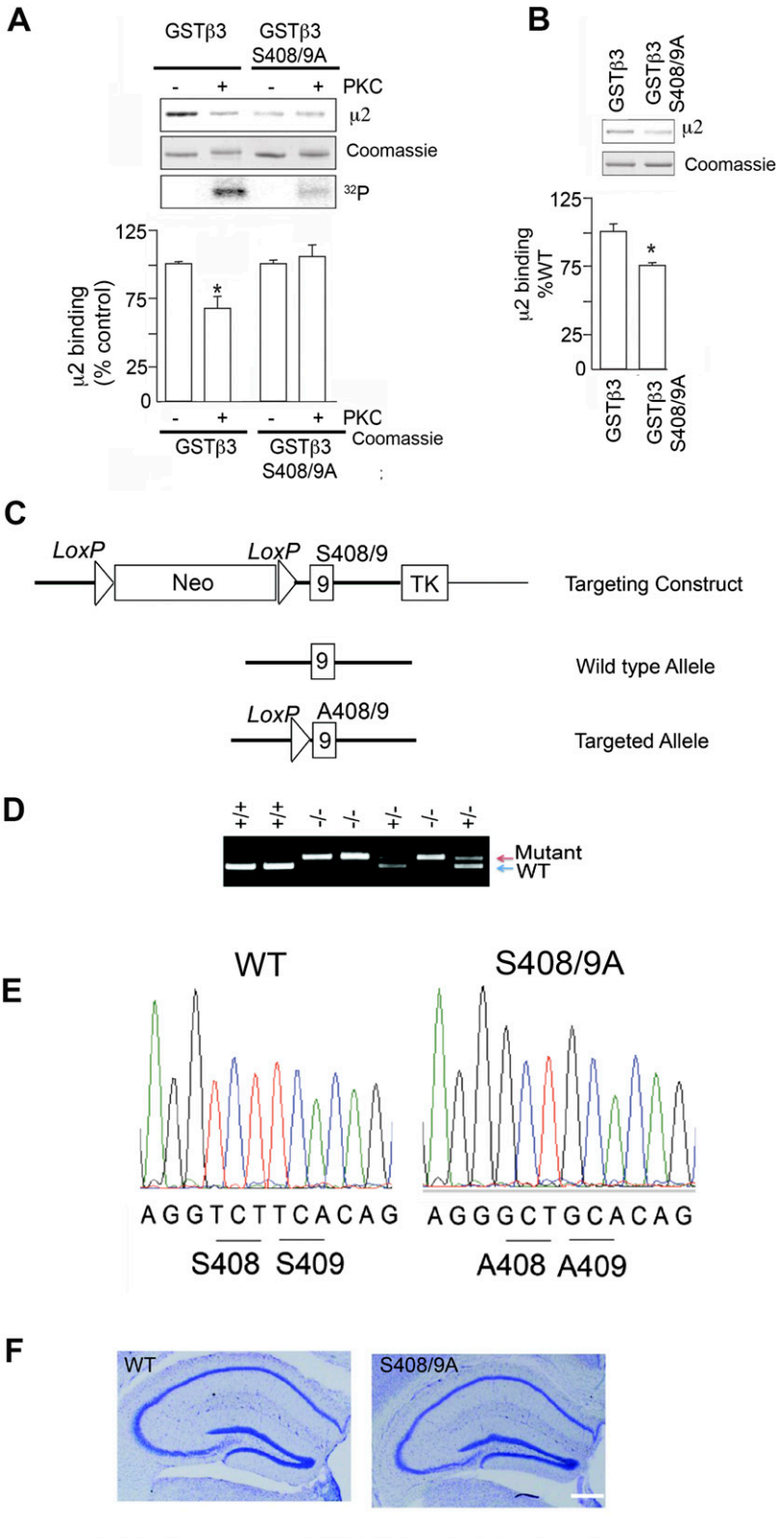

Fig. S1. Characterization of β3 phosphorylation and generation of S408/9A mice. (*A*) GST fusion proteins encoding the major intracellular domain of the β3 subunit (GST-β3) and a mutant fusion protein in which residues S408/9 were mutated to alanines (GSTβ3S408/9A) were purified from *E. coli*. Fusion proteins were subjected to in vitro phosphorylation using purified PKC. GSTβ3 was phosphorylated to 0.35 mol/mol, and GSTβ3S4089A was purified to 0.03 mol/mol. Phosphorylated fusion proteins were then exposed to brain lysates and immunoblotted with μ2 antibodies. Coomassie staining of the respective samples and an autoradiogram of samples exposed to ^{32}P–γ-ATP and PKC are shown. The level of μ2 binding was normalized to fusion proteins that had been incubated with heat-inactivated PKC. (*B*) AP2 binding to GSTβ3 and GSTβ3S408/9A was directly compared as outlined above. (*C*) Schematic diagram of the targeting

Legend continued on following page

construct for generating β3 S408/9A knock-in mice. The β3 S408/9A mice were generated by homologous recombination in ES cells. A targeting plasmid was constructed that contained a floxed neomycin (Neo) selection cassette in intron 8 of β3 genomic DNA and a flanking thymidine kinase-negative selection marker (TK). (*D*) Following Cre-mediated excision of the selection cassette in vivo, the presence of the mutant codons in exon 9 was confirmed by DNA sequencing. (*E*) PCR product of WT and β3 S408/9A DNA samples detecting the presence or absence of the remaining loxP site. (*F*) No gross morphological changes were observed in the hippocampus between WT and S408/9A mice as determined by Nissl staining. (Scale bar: 100 μm.)

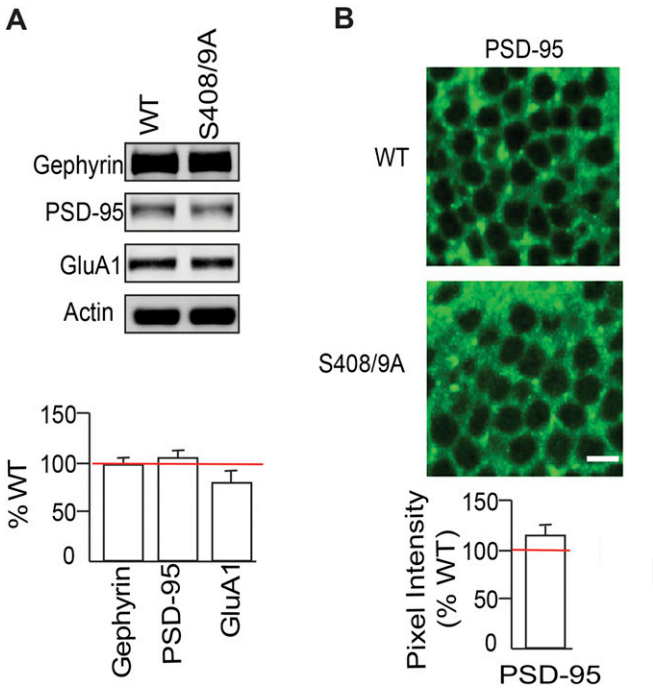

Fig. S2. Analyzing glutamate receptor expression in S408/9A mice. (*A*) Postsynaptic protein expression is unaltered in S408/9A mice. To determine whether the observed changes in inhibitory synapses were associated with alterations in postsynaptic proteins, the total expression of the inhibitory synaptic marker gephyrin, excitatory synaptic marker PSD-95, and AMPA receptor GluA1 were measured. Hippocampal lysates from S408/9A and WT control mice were subjected to SDS/PAGE and immunoblotted with gephyrin, PSD-95, and GluA1 antibodies. Protein expression in S408/9A mice was normalized to WT controls (100%; red line). No significant differences in postsynaptic protein expression were observed ($P > 0.05$, *t* test; $n = 8$ mice of each genotype). (*B*) Forty-micron hippocampal slices were stained with antibodies against the postsynaptic protein PSD-95, followed by confocal microscopy. The pixel intensity of PSD-95 staining was then compared within the dentate gyrus between genotypes. Preventing phosphorylation of the β3 subunit does not alter PSD-95 immunoreactivity ($P > 0.05$, *t* test; $n = 8$ mice of each genotype). (Scale bar: 10 μm.)

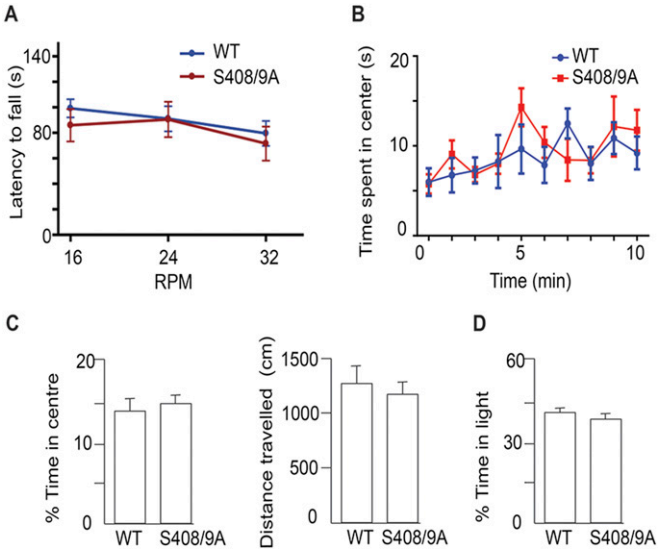

Fig. S3. Characterization of motor activity and anxiety-like behavior in S408/9A mice. (*A*) Locomotor activity of WT and S408/9A mice was examined using the rotarod test, and the latency to fall was determined. There were no significant differences in motor activity ($P > 0.05$, *t* test; $n = 10–11$ mice of each genotype). RPM, revolutions per minute. (*B*) Time spent in the center of the arena in an open field was compared for WT and S408/9A mice over a 10-min time course. (*C*) In the open-field assay, there were no significant differences in the percentage of time spent in the middle of the open-field arena or in the distance traveled between genotypes ($P > 0.05$, *t* test; $n = 12$ mice of each genotype). (*D*) Percentage of time spent in the light arena of the light/dark box assay was determined for WT and S408/9A mice. There were no significant differences in the percentage of time spent in the light arena between genotypes ($P > 0.05$, *t* test; $n = 12$ mice of each genotype).

Table S1. Comparing the excitability of DGGCs between genotypes

No. of action potentials fired in DGGCs	WT	S408/9A
Current injection amplitude, pA		
20	0.4 ± 0.4	0.0 ± 0.0
40	0.6 ± 0.5	1.0 ± 0.8
60	4.3 ± 1.8	6.9 ± 2.5
80	10.9 ± 2.9	17.1 ± 4.2
100	21.5 ± 3.5	24.5 ± 4.4
120	30.9 ± 3.6	34.0 ± 4.7
140	39.1 ± 3.6	42.6 ± 5.1
160	46.8 ± 3.8	49.7 ± 5.4
180	55.6 ± 3.8	57.9 ± 5.6
200	63.5 ± 4.3	65.0 ± 5.8
220	71.5 ± 4.6	72.2 ± 5.9
240	80.7 ± 4.7	77.5 ± 6.1
260	87.8 ± 4.9	83.2 ± 6.1
280	94.4 ± 5.0	89.5 ± 6.5
300	100.0 ± 4.9	93.6 ± 6.6
RMP, mV	−81.8 ± 1.2	−81.3 ± 1.2
I_{50}, pA	169.0	164.2
k	48.0	51.9
n	19	20

Values are mean ± SE. I_{50}, amplitude of current injection eliciting 50% of maximum response; *k*, slope factor; *n*, number of mice; RMP, resting membrane potential.